Proton-Activated Chloride Channel 1 (PACC1) is essential for innate host defense against bacterial sepsis

Lucien P Garo[1,=], Kevin Brueck[1,2,=], Sarah Walachowski[1,2], Archana Jayaraman[1], Marcel Strueve[2], Shuang Xu[1], Hulbert Yang[1], Matthew Helmkamp[1], Seung Hoan Choi[3], Christoph Reinhardt[2,4,5], Markus Bosmann[1,2*]

[1]Pulmonary Center, Department of Medicine, Boston University Chobanian & Avedisian School of Medicine, Boston, MA, 02119, USA
[2]Center for Thrombosis and Hemostasis, University Medical Center of the Johannes Gutenberg-University Mainz, Mainz, 55131, Germany
[3]Department of Biostatistics, Boston University School of Public Health, Boston, MA, 02119, USA
[4]German Center for Cardiovascular Research (DZHK), Partner Site Rhine-Main, Mainz, 55131, Germany.
[5]Research Center for Immunotherapy (FZI), University Medical Center of the Johannes Gutenberg-University Mainz, Germany.

[=]L.G. and K.B. contributed equally

***Corresponding author:**
Markus Bosmann, Associate Professor of Medicine, Pathology & Laboratory Medicine, Pulmonary Center, Department of Medicine, Boston University Chobanian & Avedisian School of Medicine, Boston, Massachusetts, 02118, USA, Phone: +1-617-358-1225, FAX: +1-617-638-5227. E-mail: mbosmann@bu.edu

Author Contributions: LG, KB, MS, and SW conducted experiments, acquired data, and analyzed data. AJ analyzed data. SX, HY, and MH assisted with conducting experiments. LG, KB, MS, and MB designed and supervised the studies. SHC shared advice regarding the genetic association data interpretation. CR contributed essential reagents, mouse strains and methods. All authors interpreted the data. MB coordinated the studies. LG wrote the manuscript with KB, AJ, and MB, which was edited by MS and CR.

Competing Interest Statement: The authors declare no competing financial interests.

Classification: Biological Sciences/Immunology and Inflammation

Keywords: Cytokines, immunology, innate immunity, infection

This PDF file includes:
Main Text
Figures 1 to 5

Abstract

Bacterial sepsis remains a devastating clinical problem. Here, we describe a protective role for the recently discovered acid-sensitive, proton-activated chloride channel, PACC1 (PAC/ASOR/TMEM206), during sepsis. Initially, we found PACC1 was enriched in healthy human and mouse mononuclear phagocytes, particularly macrophages, and differentially regulated by inflammatory stimuli, suggesting PACC1 involvement in innate immunity. To further investigate, we generated *de novo Pacc1* knockout ($^{-/-}$) mice, which presented without major immunologic abnormalities at baseline. Compared to wildtype (WT), *Pacc1*$^{-/-}$ myeloid cells showed normal phagocytic uptake of acid-insensitive *Escherichia coli BioParticles*, but impaired development of the acidifying phagolysosome using pH-sensitive *E. coli* BioParticles. Transcriptomic profiling of *Pacc1*$^{-/-}$ macrophages revealed dysregulated phagolysosomal and cytokine networks (e.g., interferons). Because phagolysosomal bacterial clearance is essential to resolve infection, we challenged *Pacc1*$^{-/-}$ mice with intraperitoneal gram-negative *E. coli* sepsis. *Pacc1*$^{-/-}$ mice displayed increased bacterial burden, immune cell infiltration, inflammation, and lethality. Additionally, gram-positive pneumococcal pneumonia was also more severe in *Pacc1*$^{-/-}$ mice, indicating broad anti-bacterial PACC1 impact. In contrast, phagocytosis-independent *E. coli* lipopolysaccharide (LPS)-induced endotoxemia yielded comparable WT and *Pacc1*$^{-/-}$ survival, as well as similar inflammatory responses. Finally, we engineered *Pacc1*-floxed ($^{fl/fl}$) mice crossed with a myeloid lineage Cre-deleter strain to interrogate myeloid cell-intrinsic PACC1 *in vivo*. Consistent with a predominate role for PACC1 during phagocytosis and bacterial clearance in these cells, *LysM-Cre/Pacc1*$^{fl/fl}$ mice exhibited impaired *E. coli* sepsis survival but indifferent endotoxemia phenotypes. In conclusion, PACC1 links sterilizing phagolysosomal activity with immune networks in sepsis pathobiology.

Significance Statement

Bacterial sepsis remains a major global health burden. Here, we report an essential role for the recently discovered acid-sensitive chloride channel, PACC1 (PAC/ASOR/TMEM206), in protective host defense during bacterial infection and sepsis. PACC1 is highly expressed in human and mouse phagocytic myeloid cells, particularly macrophages, where it regulates phagocytic bacterial clearance and inflammatory responses. Using *de novo* generated mice, we show that global or myeloid cell-targeted deletion of PACC1 impairs development of phagolysosomal acidification, confers susceptibility to bacterial infection and excessive inflammation, and undermines host defense. These findings warrant further investigation to better understand PACC1 in sepsis pathobiology.

Main Text

Introduction

Life-threatening bacterial infections are a devastating clinical problem and the molecular mechanisms of protective host defense require continued investigation. There are an estimated ~50 million cases of sepsis worldwide each year, with mortality rates of 20-50% (1). Strikingly, sepsis may account for up to 50% of US hospital deaths and is thought to be the most expensive condition affecting the US healthcare system (2, 3). Pneumonia is a major risk factor for sepsis, causing approximately 50% of all cases (4) and is itself a leading cause of death in children under five and in the elderly (5). Bacterial infections cause the majority of sepsis deaths (6), despite a recent surge in viral sepsis due to COVID-19 (7). Gram-negative *Escherichia coli* is a major pathogen of systemic bacteremia, especially in higher income countries, and the gram-positive bacterium, *Streptococcus pneumoniae*, is the most common etiology of bacterial pneumonia (8). Unfortunately, antibiotic resistance has been increasing amongst bacterial pathogens, and infection-associated mortality in the US has not significantly improved since the widespread use of antibiotics in the middle of the 20th century (6, 9). Of note, vaccines for *E. coli* are still under development and not currently available (8), while vaccines for *S. pneumoniae* provide only limited protection against certain serotypes (10). Treatment of bacterial infections is further complicated by limited diagnostic capabilities—the exact infectious microbe remains unidentified in a plurality of bacterial sepsis cases (6). Due to these ongoing public health threats, our laboratory (11-14) and many others (5, 15, 16) have been investigating broadly applicable host defense mechanisms important for innate immune responses to bacterial infections.

Tissue-resident macrophages mediate initial host defense mechanisms to invading bacterial infections and interface at mucosal/serosal sites (17). Phagocytosis by these surveilling macrophages and other myeloid cells which are rapidly recruited to the site of infection, including neutrophils and monocytes, plays a key role in preventing and limiting infection severity (18, 19). During phagocytosis,

bacteria at the plasma membrane are internalized in a receptor-mediated process into the membrane-bound phagosome, which is followed by maturation and acidification of this compartment, culminating in fusion with the highly acidic lysosome to form the phagolysosome. The strongly acidic pH of the phagolysosome and a cocktail of proteolytic enzymes kill bacteria (18, 19). Thus, the study of host defense mechanisms related to phagolysosomal development and function are of major relevance to bacterial infections.

Chloride (Cl^-) is the most abundant free anion in humans and governs biological functions ranging from intercellular signaling to intracellular vesicular acidification (20, 21). Decades of research in chloride physiology has uncovered many subtypes of cellular/intracellular membrane Cl^- channels and transporters (20). To cross cellular membranes, Cl^- requires channels for passive diffusion, or specific proteins to actively transport Cl^- in conjunction with other ions. Chloride channels/transporters have been linked to the etiology of many diseases and have been implicated as therapeutic targets in contexts including cystic fibrosis, neurodegeneration, epilepsy, osteopetrosis, hypertension, and infection (20, 21).

The molecular identity of a widely expressed acid-activated Cl^- channel, PACC1 (commonly also known as ASOR, PAC, TMEM2026) has recently been identified in two independent genome-wide siRNA screens (22, 23), validating years of electrophysiological experimental data had suggested the existence of such a channel (22-26). PACC1 channels are homotrimers of TMEM206 subunits that each contain two transmembrane domains (22, 23, 27-30). Mutagenesis and cryo-EM studies have shown that all six transmembrane domains of the trimer participate in forming a Cl^--selective pore that is open upon acid-induced contraction of their extracellular/luminal domains (22, 23, 27-30). This results in a steep pH dependence with PACC1 being closed at neutral pH and maximally activated at pH 4.5, in addition to a steep voltage dependence (22-30).

Due to its unique acid sensitivity, studies initially focused on how PACC1 promotes acid-induced cell death (22, 23, 26, 31, 32), particularly in the brain where PACC1 is highly expressed and where extracellular pH can drop during ischemic stroke (31, 32). However, beyond acidosis, the role of PACC1 in health and disease remains largely unknown.

PACC1 is ubiquitously expressed and has been detected in all mammalian cell types examined (22, 23). PACC1 is also highly evolutionarily conserved, with greater than 90% conservation between mice and humans (22, 23), suggesting involvement in essential biological functions. Beyond the established role of PACC1 in acidotoxicity, stroke, and regulating responses to extracellular acidification (22, 23, 31, 33), it's primary function may be the regulation of and ion concentrations of intracellular vesicles whose acidic pH may allow PACC1 activity (21, 34). Indeed, after its molecular identification, PACC1 has been found in endosomal compartments (22, 23, 35-38) and recent studies have identified a role for PACC1 in endosomal acidification and macropinosome resolution (35-38).

Here, we hypothesize that PACC1 plays an essential role in the phagolysosome, which constitutes an even more highly acidic compartment optimal for PACC1 activation (29), and contains one of the highest concentrations of chloride (21). We found that PACC1 in macrophages is required for effective bacterial eradication, inflammatory responses, and host resistance against sepsis.

Results

Human PACC1 is expressed abundantly in macrophages and other mononuclear phagocytes

PACC1 is ubiquitously expressed and has been detected in every cell type examined (22, 23). To explore where PACC1 may play a more predominant biological role, we first examined publicly available human single-cell RNA sequencing (scRNA-seq) data from the Human Protein Atlas (HPA) (39). The HPA scRNA-seq data was based on 31 different datasets from published studies, which were processed by the HPA team using a custom pipeline, and expression profiles were generated by normalizing read counts to normalized transcripts per million (nTPM). Amongst all cells, *PACC1* expression was highly enriched within immune cells (**Fig. 1A**). Moreover, within immune cells in peripheral blood, *PACC1* was preferentially expressed within phagocytic mononuclear myeloid cells, such as monocytes and dendritic cells, both in a dataset from the HPA (**Fig. 1B**) as well as an independent bulk RNA-seq dataset from the Immune Cell Atlas (40) (**Fig. 1C**). Within glial cells, which consist of microglia, the tissue-resident macrophage "professional" phagocytes of the brain, (as well as astrocytes and oligodendrocytes, which display some phagocytic capacity (41)), *PACC1* was also highly elevated (**Fig. 1A**). To determine whether PACC1 was also expressed in tissue-resident macrophages, the predominant mononuclear phagocytes that initially interface with bacteria during sepsis and other infections (13, 14, 16, 17, 42), we next examined all available HPA data from the 19 tissues with annotated tissue macrophage populations (**Fig. 1D**). *PACC1* was consistently enriched in immune cells compared to non-immune cells. Most strikingly, we found that tissue macrophages were the highest *PACC1*-expressing cell type in almost every tissue examined. These included Kupffer cells and Hofbauer cells, which are specialized tissue macrophages in the liver and placenta, respectively; and Langerhans cells, which are specialized tissue macrophages/dendritic cells in the skin (17). In addition, HPA bulk RNA sequencing data from 69 cell lines of various tissue origin revealed that cell lines of myeloid lineage were enriched in the top 50% in terms of ranked *PACC1* expression (***SI Appendix,* Fig. S1A**). The highest *PACC1* expression was in

THP-1 cells, and the third highest expression in U-937 cells, the most widely used cell lines for macrophage studies (43). In addition, we analyzed an expanded pool of cell lines that combined HPA bulk RNA sequencing data with data from over 1000 cell lines in the Cancer Cell Line Encyclopedia (CCLE) and a Genentech study (44). The top 2% of *PACC1*-expressing cells contained a plurality of myeloid lineage cells, including THP-1 cells (***SI Appendix,* Fig. S1B**).

To further assess whether PACC1 may be implicated in myeloid cell functions, we next analyzed *PACC1* variant data from publicly available genome-wide association studies (GWAS). Although no specific studies have functionally characterized any human *PACC1* genetic variants, we found multiple GWAS have identified *PACC1* variant associations with myeloid cell-related phenotypes. According to the Open Target GWAS aggregator (45), among all biological phenotypes associated with *PACC1* variants, myeloid cell-related phenotypes were highly represented. “Monocyte counts” ranked as the most supported phenotype among the currently available databases (**Fig. 1E**). Closer examination of these significant variant associations with myeloid cell phenotypes revealed a modest but consistent pattern: most *PACC1* variants were predicted to be loss-of-function (pLoF), and these pLoF variants were associated with greater myeloid cell counts/frequencies, whereas the few predicted gain-of-function (pGoF) variants were associated with the converse (***SI Appendix,* Table S1**). Furthermore, a large cohort from the recently available *All of Us* (AoU) dataset (46) revealed the association of septicemia with gene-level burden of low frequency *PACC1* pLoF variants (**Fig. 1F**). A separate large population cohort from the UK Biobank (47), which used a broader assortment of ICD-10 clinical codes, showed an overall modest trend in association between *PACC1* gene-level variant burden and several codes pertaining to predominantly bacterial infections (***SI Appendix,* Fig. S2**). In summary, these data demonstrate that *PACC1* expression in humans is highly enriched in mononuclear phagocytes, particularly macrophages, and that *PACC1* variants may have an impact on myeloid cell biology and infection susceptibility, suggesting that PACC1 may be involved in regulating innate immunity.

Pacc1 expression in mice is enriched in macrophages and other mononuclear phagocytes

To further evaluate PACC1 expression and potential functions in macrophages, we proceeded to investigations in mouse models. Therefore, we sought to determine whether *Pacc1* was also highly expressed in murine macrophages. Reanalysis of bulk RNA sequencing data from our previously published sepsis study (12) revealed that *Pacc1* expression was ranked in the top 5% of all detectable genes in murine bone marrow-derived macrophages (BMDMs) at baseline (**Fig. 2A**). We next asked if PACC1 was also highly enriched in macrophages vs. other immune cell types in mice. Since monoclonal antibodies for the PACC1 protein were not commercially available (48), we employed mRNA PrimeFlow (49) to specifically detect *Pacc1* mRNA across macrophage and splenocyte populations by flow cytometry. As a negative control for *Pacc1*, we leveraged cells from our *de novo* generated *Pacc1* knockout mice (***SI Appendix,* Fig. S3**), or WT cells without *Pacc1* target probe. Using this PrimeFlow approach, robust *Pacc1* expression was first confirmed in murine BMDMs (**Fig. 2B**; gating scheme in ***SI Appendix,* Fig. S4A**), as also recently confirmed at the protein level (36). Consistent with human data (**Fig. 1B-C**), *Pacc1* expression in murine splenocytes was observed in mononuclear phagocytes, including macrophages, dendritic cells, and a small population of neutrophils, as well as B cells, which also possess phagocytic capacity (19) (**Fig. 2C**; gating scheme in ***SI Appendix,* Fig. S4B**). *Pacc1* enrichment in mononuclear phagocytes was observed compared to other immune cell populations in the spleen (***SI Appendix,* Fig. S4C**). These findings were further validated by RT-qPCR in fluorescence-activated cell (FAC)Sorted splenic myeloid populations, which showed higher expression in macrophages, modest expression monocytes, and detectable expression in polymorphonuclear neutrophils (**Fig. 2D**). To ascertain PACC1 levels across a broader set of murine tissue macrophages, we analyzed published transcriptomic data comparing different macrophage populations (50). Relevant to pneumonia and sepsis, *Pacc1* was the most highly expressed in peritoneal macrophages and also highly expressed in alveolar macrophages (**Fig. 2E**), the first immune cells to interface with invading pathogens in these contexts (17). Next, we analyzed single nucleus sequencing data to examine the

peritoneal compartment more closely. *Pacc1* was highly expressed within murine macrophages and other mononuclear phagocytes, including monocytes and dendritic cells, within naïve mice (**Fig. 2F-G**). Finally, we tested if *Pacc1* in macrophages was differentially regulated in response to inflammatory stimuli associated with infection, such as Toll-like receptor (TLR) ligands. Using BMDMs, we observed that *Pacc1* expression was differentially responsive to various inflammatory stimuli (**Fig. 2H**). Of note, *Pacc1* was strongly downregulated by lipopolysaccharide (LPS), a component of gram-negative bacterial cell walls (13). Direct stimulation of macrophages with inactivated *E. coli* also inhibited *Pacc1* expression (**Fig. 2I**). Collectively, these data show that *Pacc1* expression is abundant in human and mouse macrophages, and differentially regulated by inflammatory stimuli, suggesting that PACC1 could be involved in regulating innate immune responses to infection.

De novo generation of Pacc1 knockout mice

High PACC1 levels in mononuclear phagocytes (**Fig. 1-2,** and ***SI Appendix,* Fig. S1, S4C**) suggest the possibility that PACC1 may be involved in regulating defense against infection. However, a barrier to progress in this field is the lack of commercially available *Pacc1*-deficient mice, which has led us and others to generate *Pacc1* knockout (*Pacc1*$^{-/-}$) mice (22, 23). To study the role of PACC1 *in vivo*, we generated mice with a global deletion of *Pacc1* using a CRISPR/Cas-9 approach (***SI Appendix,* Fig. S3A**). Single-guide RNAs aligned to regions flanking exon 2 of the *Pacc1* gene were injected into pronuclei/zygotes (C57BL/6J), resulting in a 120 base pair deletion with a frame shift and a premature stop codon in selected F1-generation mice. This expected truncated band was detectable by polymerase chain reaction (PCR) amplification, facilitating genotyping of these mice (***SI Appendix,* Fig. S3B**). In addition, reverse transcription quantitative-PCR (RT-qPCR) using multiple primer pairs for exons 2-8 verified the absence of productive *Pacc1* mRNA in macrophages (***SI Appendix,* Fig. S3C**), suggesting nonsense-mediated mRNA decay (51). Acid-induced cytotoxicity was lower in *Pacc1*$^{-/-}$ BMDMs confirming loss of chloride channel functioning with *Pacc1* deletion (***SI Appendix,* Fig. S3D**), further

validating previous findings from electrophysiology studies using patch-clamp recordings (25, 26, 31(25, 26). In agreement with other independently generated mouse models (22, 23), *Pacc1*$^{-/-}$ mice were viable and fertile, displaying normal sex ratio distributions, although the frequency of homozygous mice was slightly reduced to ~17% from expected Mendelian ratios (25%) in heterozygous breeding schemes (***SI Appendix,* Fig. S3E**). *Pacc1*$^{-/-}$ mice presented with no gross abnormalities. Males and females had normal body weights and normal clinical chemistry parameters including blood proteins, metabolites, and electrolytes (***SI Appendix,* Fig. S3F-I**). Importantly, *Pacc1*$^{-/-}$ mice housed under specific pathogen-free (SPF) conditions showed no apparent abnormalities in the immune compartment, with normal numbers of peripheral myeloid and lymphoid cells in the blood and spleen (***SI Appendix,* Fig. S3J-L**, gating scheme in ***SI Appendix,* Fig. S5**). Together, these data suggest that *Pacc1*$^{-/-}$ mice have no relevant developmental immunologic abnormalities, making them appropriate to study bacterial infections *in vivo*.

Pacc1$^{-/-}$ *mice have defective development of phagolysosomal acidification in vitro and in vivo*

Acid-triggered PACC1 may play an active role in the intracellular membrane of the acidifying phagolysosome of myeloid cells (29). Therefore, we first asked if bacteria induce PACC1-containing phagosomes in macrophages. To answer this, we analyzed proteomic data from Li *et al.*, which used an engineered ascorbate peroxidase (APEX)-based proximity labeling technique combined with mass spectrometry in murine macrophages to identify phagosomal host proteins following phagocytosis of APEX-tagged inactivated gram-negative *E. coli* and gram-positive *Staphylococcus aureus* (52). We identified from their datasets that PACC1 protein was enriched in bacteria-containing phagosomes with BMDMs (**Fig. 3A**). Next, we sought to test the development phagolysosomal acidification in our *Pacc1*$^{-/-}$ mice using inactivated *E. coli* BioParticles conjugated with a pH-sensitive fluorophore. These particles are phagocytosed and become fluorescent at low pH as the phagosome matures and fuses with the lysosome (53). Therefore, we stimulated acid-sensitive *E. coli* BioParticles with *Pacc1*$^{-/-}$ BMDMs *in vitro* to assess phagocytosis. BioParticles incubated with *Pacc1*$^{-/-}$ BMDMs displayed decreased fluorescence

compared to WT counterparts (**Fig. 3B**). These data appeared to indicate a defect in the development of the acidifying phagolysosome, as normal phagocytic engulfment of synthetic beads by macrophages has been reported not to require PACC1 (36), consistent with the fact that PACC1 should be inactive at the neutral plasma membrane pH (23, 27-30). We also confirmed normal phagocytic uptake of *E. coli* cargo in *Pacc1*$^{-/-}$ macrophages by exposing them to acid-insensitive Alexa Fluor (AF)488-conjugated *E. coli* BioParticles. AF488-*E. coli* emit a stable signal from pH 3-10 independent of changes in phagolysosomal acidification (54). AF488 fluorescence in *Pacc1*$^{-/-}$ macrophages was indistinguishable from WT, and signals in both strains were abrogated by cytochalasin D, an inhibitor of actin polymerization commonly used to inhibit phagocytic uptake (54, 55) (**Fig. 3C-D**). Accordingly, *Pacc1*$^{-/-}$ macrophages showed less efficient intracellular killing of live pathogenic *E. coli* in cell culture, while levels of extracellular bacteria were identical to those in WT cultures (**Fig. 3E**), consistent with normal phagocytic uptake by *Pacc1*$^{-/-}$ macrophages followed by defects in downstream phagolysosomal bacterial killing. When acid-sensitive *E. coli* BioParticles were injected intraperitoneally (i.p.), we observed a similar reduction in fluorescence in *Pacc1*$^{-/-}$ myeloid cells (**Fig. 3F-G**). Additionally, signs of greater inflammation were observed in *Pacc1*$^{-/-}$ mice in response to these inactivated BioParticles, including an overall greater recruitment of myeloid cells to the peritoneum, including monocytes and monocyte-derived macrophages (**Fig. 3H**, gating scheme in ***SI Appendix,* Fig. S6**). We also observed elevated release of IL-6, a well-studied pro-inflammatory cytokine in sepsis and pneumonia (13), in peritoneal lavage fluid in these *Pacc1*$^{-/-}$ mice injected with BioParticles (**Fig. 3I**). In contrast, in naïve *Pacc1*$^{-/-}$ mice, we found no aberrant signs of pre-existing inflammation in the peritoneum at baseline (***SI Appendix,* Fig. S7**), consistent with immunoprofiling in the periphery (***SI Appendix,* Fig. S3J-L**). Like WT, naïve *Pacc1*$^{-/-}$ mice displayed low levels of infiltrating peritoneal monocytes and neutrophils, (including a modestly lower level of monocytes) (***SI Appendix,* Fig. S7A-B**), and undetectable levels of IL-6 (***SI Appendix,* Fig. S7C**). As a whole, these data suggest acidification of the phagolysosome is defective in *Pacc1*$^{-/-}$ myeloid cells, and that PACC1 deficiency may result in hyperinflammation following bacterial challenge.

Pacc1$^{-/-}$ macrophages have dysregulated immunologic and phagolysosomal transcriptomic responses

To screen for the transcriptome-wide effects of *Pacc1* loss on host defense and phagolysosomal pathways, we performed RNA sequencing of BMDMs stimulated with *E. coli* BioParticles. Principal component analysis revealed strong segregation of groups based on *E. coli* stimulation, as well as segregation based on genotype (**Fig. 4A**). *Pacc1$^{-/-}$* control compared to WT control samples were distinguishable at baseline and further segregated following phagocytic stimulation. *E. coli* triggered robust transcriptomic activity, with >10,000 significantly differentially expressed genes (DEGs) in each group of WT and *Pacc1$^{-/-}$* macrophages (***SI Appendix,* Fig. S8A-C; Dataset S1**). In response to *E. coli* challenge, *Pacc1$^{-/-}$* vs. WT macrophages displayed 2,162 upregulated DEGs and 1,795 downregulated DEGs (**Fig. 4B**). WT and *Pacc1$^{-/-}$* macrophages also displayed a smaller proportion of DEGs at baseline (***SI Appendix,* Fig. S8D**); however, the majority of DEGs were uniquely dysregulated in response to *E. coli* challenge (**Fig. 4C**).

First, to assess global changes in functional pathways, we performed a gene set enrichment analysis (GSEA) for hallmark biological processes using both significant and non-significant DEGs. Immunological gene sets were differentially enriched in *Pacc1$^{-/-}$* vs. WT macrophages both at baseline (***SI Appendix,* Fig. S9A; Dataset S2**) and following *E. coli* phagocytosis (**Fig. 4D; *SI Appendix,* Dataset S2**), including tumor necrosis factor (TNF)-α via nuclear-factor κ b (NFκb) signaling (***SI Appendix,* Fig. S9B-C**) and interferon responses (***SI Appendix,* Fig. S9D-G**), as well as overall JAK/STAT signaling (***SI Appendix,* Fig. S9A, H**). Broader analysis via the "Interferome database", a curated list of empirically determined interferon-responsive genes (56), revealed strong dysregulation of type I and type II interferon signaling in *Pacc1$^{-/-}$* macrophages following bacterial challenge (***SI Appendix,* Fig. S10**).

We also performed Ingenuity Pathway Analysis (IPA) to identify dysregulated gene sets in *Pacc1$^{-/-}$* macrophages in response to *E. coli* (***SI Appendix,* Dataset S3**). IPA found alterations in multiple immunologic pathways; notably the "pathogen-induced cytokine storm signaling pathway" was one of the most highly upregulated pathways in *Pacc1$^{-/-}$* compared to WT macrophages (**Fig. 4E**). Uncontrolled

cytokine storm is thought to be a leading contributor to death in sepsis patients (16). Examination of the DEGs enriched in this pathway resolved that this activation response was not uniform: expression of some inflammatory mediators were elevated in *Pacc1*$^{-/-}$ macrophages relative to WT following exposure to *E. coli* BioParticles (e.g., *Il1rap, Ccl6*, *Pf4, Ripk1, Jak1, Stat3, Tlr9, Tlr3, Cgas, Nod1,* and *Sting1*), while others were downregulated (e.g., *Il6*, *Il1b*, *Cxcl1*, *Cxcl2*, and *Il12b*).

Next, to study dysregulated biological processes in *Pacc1*$^{-/-}$ macrophages at a more granular level, including phagolysosomal functions, we analyzed the enrichment of gene ontology biological processes (GOBPs) for significant DEGs (***SI Appendix,* Dataset S4**). Amongst the top upregulated GOBPs, a majority were associated with either innate immunity or intracellular vacuoles/vesicles (**Fig. 4F**). More than 100 DEGs were enriched in "regulation of innate immune response" processes in *Pacc1*$^{-/-}$ vs. WT macrophages, the majority of which were associated with positive regulation of innate immune response, both following *E. coli* incubation and at baseline (***SI Appendix,* Fig. S11**). In contrast, the top downregulated pathways in *Pacc1*$^{-/-}$ vs. WT macrophages during phagocytosis were not directly related to immunologic responses, but related predominantly to RNA processing (***SI Appendix,* Fig. S12**).

To determine if *Pacc1* loss affected downstream phagolysosomal regulation, we manually curated a list of the respective annotated processes. Consistent with an important role for PACC1 during bacterial challenge, multiple GOBPs associated with lysosomal activity were significantly differentially regulated in *Pacc1*$^{-/-}$ vs. WT macrophages (e.g., lysosomal organization/transport, lysosomal lumen acidification; adj. $P<0.1$), while differences GOBPs associated with early phagocytic processes (e.g., engulfment) were not significant (**Fig. 4G**). Interestingly, a majority of the DEGs enriched in these phagolysosomal processes were upregulated (**Fig. 4H**), which may indicate a potential transcriptomic compensatory response for the defective phagolysosomal acidification we observed in *Pacc1*$^{-/-}$ macrophages (**Fig. 3B-G**). A subset of phagolysosomal processes were also dysregulated at baseline in *Pacc1*$^{-/-}$ compared to WT macrophages (***SI Appendix,* Fig. S13**) suggesting previously unexpected residual activity of this ion channel in resting cells. In summary, these data indicate that loss of *Pacc1* in macrophages results in

transcriptomic dysregulation in immunological and phagolysosomal pathways, particularly in response to phagocytotic bacterial stimulus.

Pacc1 knockout mice and myeloid cell-targeted conditional Pacc1 knockout mice are susceptible to E. coli sepsis.

Because it is well known that defective phagolysosomal acidification inhibits pathogen clearance (18, 19), we next studied if *Pacc1*$^{-/-}$ mice were susceptible to bacterial infections. Using a well-established *E. coli* sepsis model (12), mice were injected with 2x10^{8} colony forming units (CFUs) of *E. coli* i.p. (**Fig. 5A**). We found that *Pacc1*$^{-/-}$ mice succumbed to severe mortality during the observation period of 10 days after infection (**Fig. 5B**). In contrast to 100% of WT counterparts, only about 50% of *Pacc1*$^{-/-}$ mice survived. This increased lethality was associated with significantly higher bacterial burden in the peritoneal lavages (**Fig. 5C**) and systemic bacteremia (**Fig. 5D**, gating scheme in ***SI Appendix,* Fig. S14A**). Moreover, *Pacc1*$^{-/-}$ mice displayed a greater inflammatory response in terms of myeloid cell infiltration (**Fig. 5E,** gating scheme in ***SI Appendix,* Fig. S14B**) and release of proinflammatory IL-6 in peritoneal lavage fluid (**Fig. 5F**). However, this enhanced compensatory response was apparently unable to clear infection. In conclusion, these data suggest *Pacc1*$^{-/-}$ mice are susceptible to bacterial infection and dysregulated inflammation, which may be explained by defective myeloid cell responses.

Next, to test whether this susceptibility of *Pacc1*$^{-/-}$ mice to a gram-negative bacterial infection in the peritoneum (**Fig. 5A-F**) was also applicable to other pathogens, we performed additional experiments using a gram-positive pneumococcal pneumonia model in the lung (57). Mice were intranasally (i.n.) inoculated with 1-2x10^{6} CFUs of S. *pneumoniae*, serotype 4 (SPN4) (***SI Appendix,* Fig. S15A**). As with *E. coli* sepsis, *Pacc1*$^{-/-}$ mice experienced significantly greater mortality (***SI Appendix,* Fig. S15B**), as well as greater peak weight loss (***SI Appendix,* Fig. S15C**) and lung injury (***SI Appendix,* Fig. S15D**) as indicated by total protein leakage into the bronchoalveolar space from bicinchoninic acid assay.

Accordingly, *Pacc1*$^{-/-}$ mice tended to have a higher bacterial burden (***SI Appendix,* Fig. S15E**). Similar to *E. coli* sepsis, pneumococcal pneumonia induced more pronounced local myeloid cell infiltration as noted in bronchoalveolar lavages from *Pacc1*$^{-/-}$ mice (***SI Appendix,* Fig. S15F**, gating scheme in **Fig. S16**). This was accompanied by a general elevation of inflammatory cytokines and chemokines (***SI Appendix,* Fig. S15G-H**), including IL-6 as well as IFN-γ, a cytokine important for macrophage activation and bacterial clearance (5, 16, 58). In contrast, we found no signs of inflammation in the lung at baseline in naïve *Pacc1*$^{-/-}$ mice (***SI Appendix,* Fig. S17**), which was consistent with immunoprofiling in other sites (***SI Appendix,* Fig. S3J-L, S7**). We observed an elevation in homeostatic numbers of alveolar macrophages in *Pacc1*$^{-/-}$ mice (***SI Appendix,* Fig. S17A-B**), which could represent a potential compensatory response for phagocytic defects of *Pacc1*$^{-/-}$ alveolar macrophages. Like WT, naive *Pacc1*$^{-/-}$ mice displayed low levels of infiltrating peritoneal monocytes and neutrophils (***SI Appendix,* Fig. S17A-B**), and undetectable levels of IL-6 (***SI Appendix,* Fig. S17C**). Overall, these data suggest that *Pacc1*$^{-/-}$ mice are susceptible to bacterial infection and trigger hyperinflammation associated with defective myeloid cells in this context.

We asked if the severe mortality and inflammation in septic *Pacc1*$^{-/-}$ mice was dependent on phagocytosis or if it could be triggered by other intrinsic aberrant hyperinflammatory signaling resulting from *Pacc1* deficiency. Therefore, we also tested a sterile model of endotoxemia via i.p. injection of *E. coli*-derived LPS (**Fig. 5G**). In contrast to live *E. coli*, LPS activates TLR4 without phagocytic uptake (13). A high dose of LPS resulted in 100% mortality within four days (**Fig. 5H**), while a medium dose of LPS led to approximately 50% mortality over the observation period (**Fig. 5I**). The survival curves for *Pacc1*$^{-/-}$ vs. WT mice were nearly identical at both titrations, indicating that PACC1 is not required for phagocytosis-independent inflammatory responses. Consistently, IL-6 concentrations were comparable between *Pacc1*$^{-/-}$ and WT mice (**Fig. 5J**). Transcription in *Pacc1*$^{-/-}$ BMDMs following LPS stimulation *in vitro* also revealed indistinguishable responses from WT (***SI Appendix,* Fig. S18**).

Although *PACC1* is enriched in macrophages (**Fig. 1-2**), *PACC1* expression remains ubiquitous (**Fig. 1**), making it challenging to definitively assign a causal role to PACC1 in macrophages during bacterial sepsis in mice. Therefore, to evaluate PACC1 loss in specific cell types during *in vivo* infection, we initiated the *de novo* generation of *Pacc1*$^{fl/fl}$ mice via a CRISPR/Cas9 approach (**Fig. 5K**). The expected elongated bands in *Pacc1*$^{fl/fl}$ mice that received loxP insertions were detectable by PCR amplification, facilitating genotyping of these mice (***SI Appendix,* Fig. S17A**). As expected, *Pacc1*$^{fl/fl}$ mice showed unchanged *Pacc1* expression in peritoneal cells before Cre-mediated recombination (***SI Appendix,* Fig. S17B**). *Pacc1*$^{fl/fl}$ mice were then crossed with *LysM-Cre* mice (59) for targeted deletion of *Pacc1* within myeloid lineage cells, resulting in >90% deletion in peritoneal tissue macrophages (**Fig. 5L**, gating scheme in ***SI Appendix,* Fig. S17C**). Crucially, these conditional knockout mice recapitulated the high sepsis mortality seen in global *Pacc1*$^{-/-}$ (**Fig. 5M**), which was similarly associated with greater bacterial burden in the peritoneum (**Fig. 5N**). We also examined if *LysM-Cre/Pacc1*$^{fl/fl}$ mice showed identical responses to littermate controls during endotoxemia, employing a lower dose of LPS to detect potentially subtle differences in sensitivity. Myeloid cell-targeted *Pacc1* deletion had no discernable impact on survival (**Fig. 5O**) or peripheral blood and immune cell parameters (**Fig. 5P-Q**) during endotoxemia, further implicating a role for PACC1 in phagocytosis-mediated immunity. In conclusion, these data suggest that PACC1 promotes protective host responses, as PACC1 loss within myeloid cells undermines anti-bacterial defense mechanisms and weakens resistance to both gram-negative and gram-positive bacterial pathogens in sepsis and pneumonia.

Discussion

Bacterial sepsis remains a major global health burden (1). Our study has identified the recently discovered acid-sensitive chloride channel, PACC1 (also known as PAC, TMEM206, and ASOR) (22, 23), as a critical regulator of host defense against bacterial infections that lead to sepsis. PACC1 was highly expressed within human and mouse phagocytic myeloid cells, particularly macrophages, where it controlled sepsis outcomes. Using *de novo*-generated mice, we showed that loss of *Pacc1* globally or in myeloid cells impaired development of phagolysosomal acidification, conferred susceptibility to bacterial infection and excessive inflammation, and undermined host defense.

While PACC1 is unique in that it is activated under highly acidic conditions, the ubiquitous expression of PACC1 has obscured its physiological functions (22, 23). The data we have presented showing elevated *PACC1* expression in human and murine macrophages, along with GWAS data linking *PACC1* variants with various myeloid cell phenotypes, suggest an important role for PACC1 in macrophage responses. Our re-analysis of the proteomic data from Li *et al.* (52) confirmed that PACC1 localized to bacteria-containing phagosomes in primary macrophages, although the lack of reliable, commercial monoclonal PACC1 antibodies constrained further experimental detection at the protein level (48). These data are consistent with findings in other model systems elucidating PACC1 expression using either in-house generated PACC1 antibodies or artificial PACC1 reporter insertions in cell lines (33, 35, 36). In human HEK293 cells, PACC1 colocalizes with early endosomal markers and to a lesser extent with the lysosomal marker, LAMP-1 (36). Recent data further demonstrate that PACC1 translocates from the plasma membrane to intracellular compartments via a YxxF trafficking motif (35). In BMDMs, PACC1 has similarly been shown to colocalize more with early endosomal markers and to a lesser extent with the late endosomal marker, RAB7, or LAMP-1 (36). These studies, especially those directly in BMDMs rather than cell lines, support that PACC1 expression in the macrophage phagolysosome is the result of PACC1 from the plasma membrane accompanying subsequent vesicular development and fusion. Most recently, consistent with our findings in BMDMs, PACC1 upregulation has been reported in bone marrow-

differentiated osteoclasts, a specialized type of multi-nucleated macrophage capable of bone resorption (33). In addition, our findings explicitly identified elevated *Pacc1* expression in murine tissue macrophages and other physiologic primary immune cells differentiated *in vivo.*

Our data also showed that *Pacc1* expression in macrophages was dynamically regulated in response to diverse inflammatory stimuli related to infection, including TLR ligands. This suggests a context-specific role for PACC1 in infection, potentially adapting its function to the local inflammatory milieu. For example, downregulation of PACC1 at the plasma membrane may mediate cellular adaptation and survival to extracellular acidic environments following infection-associated inflammation (22, 23, 31, 32).

The data presented here indicate that PACC1 promotes the development of phagolysosomal acidification, as *Pacc1*$^{-/-}$ myeloid cells were less able to induce fluorescence from phagocytosed acid-sensitive *E. coli* BioParticles, and consequently less efficient at killing live *E. coli*. Our conceptual view that PACC1 is essential for microbial phagocytosis and other related endocytic, exocytic, and pinocytic processes is shared by others (33, 35-38, 60). The contextual outcomes of *Pacc1* loss may depend on the specific cell types and pathogens/cargos examined, as well as independently engineered *Pacc1*-deficient mouse strains. For example, while PACC1 may limit endosomal acidification during transferrin recycling in cell lines and certain receptor trafficking in neurons (35, 37), we found that PACC1 facilitates acidification in macrophage phagolysosomes. This may occur via the influx of chloride that is postulated to serve as an electrical shunt that permits proton pumping by vacuolar H^+ (V-)ATPase to drive acidification (21, 34). PACC1 has been well-characterized as being strongly outwardly rectifying (22-30). However, PACC1 is a passive channel, not an active directional transporter, and thus chloride loading into the lumen would depend on the contextual electrochemical gradient. Of note, the role of chloride in vesicular acidification and the anion shunt hypothesis remain controversial (21). Several studies have suggested that chloride influx is dispensable for lysosomal acidification (61, 62), while chloride may also serve important biological functions outside of its role as an anion shunt (21). In terms of vesicular acidification, there is even ambiguity around the most well-studied chloride channel, cystic fibrosis

transmembrane conductance regulator (CFTR). Multiple independent groups have reported that CFTR is required for the proper acidification of intracellular organelles, while others have shown no effect of CFTR on acidification and bacterial clearance in macrophages (21, 34, 63, 64). Reviews of the literature have suggested several inconclusive explanations, including differences in CFTR knockdown, knockout, pharmacological inhibition, or mutations; differences in human and mouse primary macrophages and cell lines; and other differences in experimental protocols, models, and modalities (21, 34, 63, 64). Most recently, Badr *et al*. have suggested that the type of bacteria or phagocytic cargo is critical, as macrophages from cystic fibrosis patients were found to have defective lysosomal acidification following phagocytosis of *Burkholderia cenocepacia*, but not of *E. coli* (65). In conclusion, further work is needed to clarify the nuanced context-dependent role of chloride in vesicular acidification, as well as the specific biophysical mechanisms undermining the development of the acidifying phagolysosome in *Pacc1*$^{-/-}$ macrophages.

In the present study, transcriptomic profiling of *Pacc1*$^{-/-}$ macrophages exposed to *E. coli* BioParticles revealed dysregulated immunologic functions. Consistent with our hypothesis that PACC1 is critical in phagolysosomal activity, lysosomal processes were amongst the most highly dysregulated pathways in *Pacc1*$^{-/-}$ macrophages; while processes associated with earlier phagocytic events less dependent on lysosomal acidification (e.g., initial engulfment) were largely unaffected. However, an unexpected observation was the upregulation of lysosomal-related processes in *Pacc1*$^{-/-}$ macrophages. In contrast, we observed defective phagolysosomal activity using acid-sensitive pHrodo *E. coli* BioParticles *in vitro,* along with corresponding host defense impairments during live bacterial infection *in vivo*. It is possible this upregulation of lysosomal processes at the transcriptomic level represents a compensatory response. RNA sequencing in *Pacc1*$^{-/-}$ macrophages also revealed enhanced signaling from endolysosomal TLRs that respond to stimuli from phagocytosed bacteria (18, 19). These findings raise the possibility that impaired phagolysosomal acidification resulted in inefficient cargo degradation that extended ligand–receptor contact. Indeed, other reports have posited the same “extended contact” hypothesis (66), acknowledging that while a degree of acidification is required for proper endolysosomal

TLR ligand binding and activation (67), partial defects in macrophage phagolysosomal acidification can result in enhanced endolysosomal TLR signaling (66). In addition, *Pacc1*$^{-/-}$ macrophages showed global innate immunologic dysregulation in processes intertwined with but less directly dependent on phagolysosomal processes, such as upregulation of interferon responses and signaling of some TLRs expressed predominantly at the plasma membrane but which can be trafficked to endosomal membranes (13, 18, 68). Notably, innate immune activation in *Pacc1*$^{-/-}$ macrophages was heterogenous, with both positive and negative regulation of various inflammatory cytokines and chemokines. The observed heterogeneity in cytokine responses indicates that PACC1 may differentially regulate distinct inflammatory pathways via mechanisms that deserve further studies in future.

Unexpectedly, we found *Pacc1*$^{-/-}$ macrophages displayed transcriptomic perturbations even at baseline, despite the absence of overt immunologic abnormalities in the myeloid compartment in naive mice (22, 23, 33). This may reflect homeostatic phagocytic activity, such as efferocytosis (17-19), or possibly non-canonical signaling roles for PACC1 (48, 69-75), as has been described for other intracellular chloride channels (76, 77). To date, PACC1 functional studies have focused primarily on its direct electrophysiological regulation of chloride conductance (22, 23, 27-29, 31, 35, 36, 78).

Interestingly, we observed some differential inflammatory responses between *Pacc1*$^{-/-}$ vs. WT BMDMs challenged *in vitro* with inactivated *E. coli* BioParticles compared to mice *in vivo* after live or inactivated bacteria (e.g. IL-6 production). This may be due to differences from tissue macrophage populations, differences from live infection and bacterial burdens in WT vs. *Pacc1*$^{-/-}$ mice, as well as differences from the inflammatory milieu *in vivo* such as the contributions of infiltrating myeloid cells. *Pacc1* deficiency had no impact on LPS-induced inflammation, including IL-6 production, and did not affect low baseline IL-6 levels in the blood or alveolar or peritoneal spaces. The present findings support the idea that the elevated IL-6 observed in *Pacc1* $^{-/-}$ mice challenged with bacteria reflects the particular *in vivo* inflammatory context rather than a baseline discrepancy in macrophage-intrinsic responses.

The predominant impact of PACC1 during sepsis appeared to be associated with phagocytosis. Endotoxemia, which (as mentioned above) activates TLR4 independent of phagocytosis (13), resulted in

Pacc1$^{-/-}$ survival comparable to that of WT mice. Conversely, in line with impaired phagolysosomal acidification, *Pacc1*$^{-/-}$ mice exposed to intact live bacterial cargo exhibited increased bacterial burdens and susceptibility to sepsis. The augmented neutrophil recruitment in *Pacc1*$^{-/-}$ mice may have served as a compensatory response when tissue-resident macrophages failed to control bacterial pathogens during early infection (5, 16). Although heightened inflammation likely reflects increased bacterial burden, *Pacc1*$^{-/-}$ myeloid cells also displayed intrinsic hyperresponsiveness to bacterial challenge, as evidenced by exaggerated cytokine responses to inactivated *E. coli*. The translational relevance of these findings was supported by congruence with human genetic data. Predicted loss-of-function *PACC1* variants were associated with increased myeloid cell counts and risk for septicemia and various bacterial infections, reflecting the phenotype observed in *Pacc1*$^{-/-}$ mice during live infection.

The susceptibility to bacterial sepsis in our conditional myeloid cell-targeted *LysM-Cre*/*Pacc1*$^{fl/fl}$ knockout mice validated an intrinsic role for PACC1 in these cells in mediating response to live infection. In contrast, outcomes to endotoxemia were unaltered in *LysM-Cre*/*Pacc1*$^{fl/fl}$ mice. The presented findings were consistent with the interpretation that PACC1 may mediate phagolysosomal bacterial clearance via action within macrophages, monocytes and neutrophils. Indeed, *Pacc1*$^{-/-}$ neutrophils also exhibited defective development of the acidifying phagolysosome in response to *E. coli* BioParticles *in vivo*. Although PACC1 expression is greater in mononuclear phagocytes, which are the first professional innate immune cells to encounter invading pathogen, neutrophils quickly become the predominant cell type during infection following their infiltration to the site of infection (5, 17). Future studies may further elaborate on the direct role of PACC1 in other PACC1-expressing immune cells in addition to macrophages.

An important unanswered question is whether augmenting PACC1 function could provide therapeutic benefit in sepsis. To date, limited studies have been conducted in engineered PACC1-overexpressing cell lines *in vitro* (22, 60, 79, 80). Unfortunately, there are currently no known specific PACC1 agonists (or antagonists) to test the translational relevance of augmenting PACC1 therapeutically in mice (79).

In parallel to our work, Cheng *et al.* also recently studied the role of PACC1 in macrophages and infection (60). Both studies suggest PACC1 is crucial for phagolysosomal acidification, bacterial clearance, inflammation, and sepsis susceptibility (60). Both indicate PACC1 is abundant in macrophages and downregulated by LPS, with *Pacc1*$^{-/-}$ macrophages showing increased interferon signaling and other inflammatory responses following bacterial challenge, though no change in inflammatory transcripts after LPS exposure (60). Although Cheng *et al.* suggest that enhanced acidification during phagocytosis releases more bacterial ligands (60), partial defects in acidification may also enhance TLR signaling due to extended ligand contact (65).

While our study characterized defective phagolysosomal acidification, decreased survival, and hyperinflammation in *Pacc1*$^{-/-}$ mice *in vivo* following bacterial infection, Cheng *et al.* reported the converse (60). These differences may arise from factors such as distinct mouse strains, pathogen differences, and experimental methods. For example, we employed global *Pacc1*$^{-/-}$ and *Pacc1-floxed* mice independently generated from those used by Cheng *et al.* (60), with strict controls to minimize microbiome variability and ensure genetic consistency (81, 82). Given that PACC1 is evolutionarily conserved (22, 23), we speculate that PACC1 may be a target of microbial evasion strategies and that bacterial pathogenicity factors could modulate its activity, potentially explaining the *E. coli* strain-dependent differences between studies (60). As discussed above, we have confirmed our findings using both a gram-negative *E. coli* peritoneal infection model and a gram-positive *S. pneumoniae* lung infection model, supporting relevance across distinct bacterial contexts in mice. Our experimental findings were also supported by congruence with human genetic variant data linking predicted loss-of-function *PACC1* variants with increased myeloid cell counts and risk for septicemia and various bacterial infections. Discrepant results may also stem from differences in cell types, time points, and cargo, especially since Cheng *et al*. used zymosan-conjugated particles (60), while we employed *E. coli*. The type of cargo has been shown to significantly impact phagolysosomal acidification related to chloride trafficking (64).

Again, the role of chloride traffickers in phagolysosomal acidification is still debated (21, 34, 61-65), and PACC1 functions are complicated by its context-dependent behavior as a passive channel. For example, recent work suggests PACC1 may increase acid-induced cell death in colorectal cancer cells (68, 69), diverging from previous findings by us and others (22, 23, 26, 31, 32). Additionally, PACC1 may have non-canonical roles in cell signaling, which could influence experimental outcomes (70). This may include direct protein binding partners independent of chloride (48, 69), which is in line with other chloride channels as mentioned above (76, 77). PACC1 has been implicated in opposing cancer cell processes like proliferation and migration (70-74), and recent data suggest it may function at non-acidic pH in aged *Pacc1*$^{-/-}$ mice that present with ophthalmic pathology (75). Interestingly, both our findings and those of Cheng *et al.* (60) reveal dysregulation of RNA processing pathways in *Pacc1*$^{-/-}$ macrophages, although the precise role of chloride channels in RNA processing remains undefined. In total, findings from our current study and prior research will help to advance the understanding of the multi-faceted roles of PACC1.

In conclusion, our results demonstrate a novel role for PACC1 in protective host defense and warrant further studies on PACC1 during sepsis and other life-threatening bacterial infections that continue to pose a major disease burden worldwide.

Materials and Methods

All the materials used in this study including sources for antibodies and reagents, and detailed methodology for the generation of mouse strains, BMDM isolation and assays, analysis of splenocytes and blood, *E. coli* BioParticle assays, live *E. coli* sepsis, pneumococcal pneumonia, endotoxemia, flow cytometry, protein detection and ELISAs, RT-qPCR, bulk and single cell/nucleus transcriptomics, proteomics, and GWAS datasets, as well as all statistical analyses, are described in the ***SI Appendix***, Materials and Methods. In brief, *Pacc1*$^{-/-}$ mice (C57BL/6J-*Pacc1*^{em1Bosm}/Bosm, MGI: 6283429) were generated *de novo* by CRISPR/Cas9-mediated gene editing at the Johannes Gutenberg University Mainz, Germany. *Pacc1*$^{fl/fl}$ mice (C57BL/6J-*Pacc1*^{em2Bosm}/Bosm, MGI: 7703212, JAX stock No.: 039760) mice were generated by Biocytogen (Beijing, China) using CRISPR/Cas9-based extreme genome editing (EGE^{TM}) technology. WT C57BL/6J and *LysM-Cre* (B6.129P2-*Lyz2*$^{tm1(cre)Ifo}$/J) mice were originally obtained from Jackson Laboratories and subsequently bred at our institutions under co-housing conditions with *Pacc1* strains, allowing the generation and use of Cre-lox littermates for experimental comparisons. All animal studies were approved by the State Investigation Office of Rhineland-Palatinate and the Institutional Animal Care and Use Committee (IACUC) of Boston University.

Acknowledgments

This work was supported by the Federal Ministry of Education and Research (01EO1503 to MB), the Deutsche Forschungsgemeinschaft (BO3482/3-3, BO3482/4-1 to MB), the National Institutes of Health (1R01HL141513, 1R01HL139641, 1R01HL166588 to MB; F31HL176388-01A1 to LG; and 5T32HL007035-50 which supported the training of LG). CR is a scientist at the German Center for Cardiovascular Research (DZHK). CR is a member of the DFG Research Unit 5644 INFINITE (RE 3450/15-1), the Center for Translational Vascular Biology (CTVB), the Research Center for Immunotherapy (FZI), and the Potentialbereich EXPOHEALTH at the Johannes Gutenberg-University

Mainz. CR was awarded a Fellowship from the Gutenberg Research College at the Johannes Gutenberg-University Mainz. We cordially thank Dr. Thomas J. Jentsch for collaborative efforts and Dr. Kara Vasilew for assistance. We also thank the Flow Cytometry Core Facility of Boston University School of Medicine (S10 OD038346) and Shari Brezinsky for assistance. The authors are responsible for the contents of this publication.

Data, Materials, and Software Availability

Single nucleus multiome (RNA and ATAC) sequencing data from our previous study has been deposited in the NCBI Gene Expression Omnibus (GEO) repository under accession code GSE269703 (reviewer access token: wbcxyyaahfandwz). Only data pertaining to unstimulated cells were used for this study. The bulk RNA-seq data generated in this study is available in GEO with the accession code GSE292930 (reviewer access token: yjinyuiihnyjpep). Phenotypes associated with human *PACC1* variants were retrieved from the Open Targets Platform (https://platform.opentargets.org/) (45). Genetic association data for *PACC1* variants in the All of Us Biobank were retrieved from the browser by Jurgens *et al.* (https://hugeamp.org:8000/research.html?pageid=600_traits_app_home) (46). Data for *PACC1* variants within the UK Biobank were retrieved from Genebass (https://app.genebass.org/) (47). *PACC1* expression from single-cell RNA sequencing data from human tissues and bulk RNA sequencing data from human cell lines were retrieved from the Human Protein Atlas (https://www.proteinatlas.org/) (39). Data from the published studies by Roewe *et al.* (12), Qie *et al.* (50), and *Li et al.* (52) were retrieved from the source data or supplementary data of the publications. *PACC1* normalized expression counts were from the Immunological Genome Project Immune Cell Atlas (http://immunecellatlas.net/ICA_Skyline.php) (40). This paper does not report original code. Any additional information required to reanalyze the data reported herein is available from the corresponding author upon request.

Figures and Captions

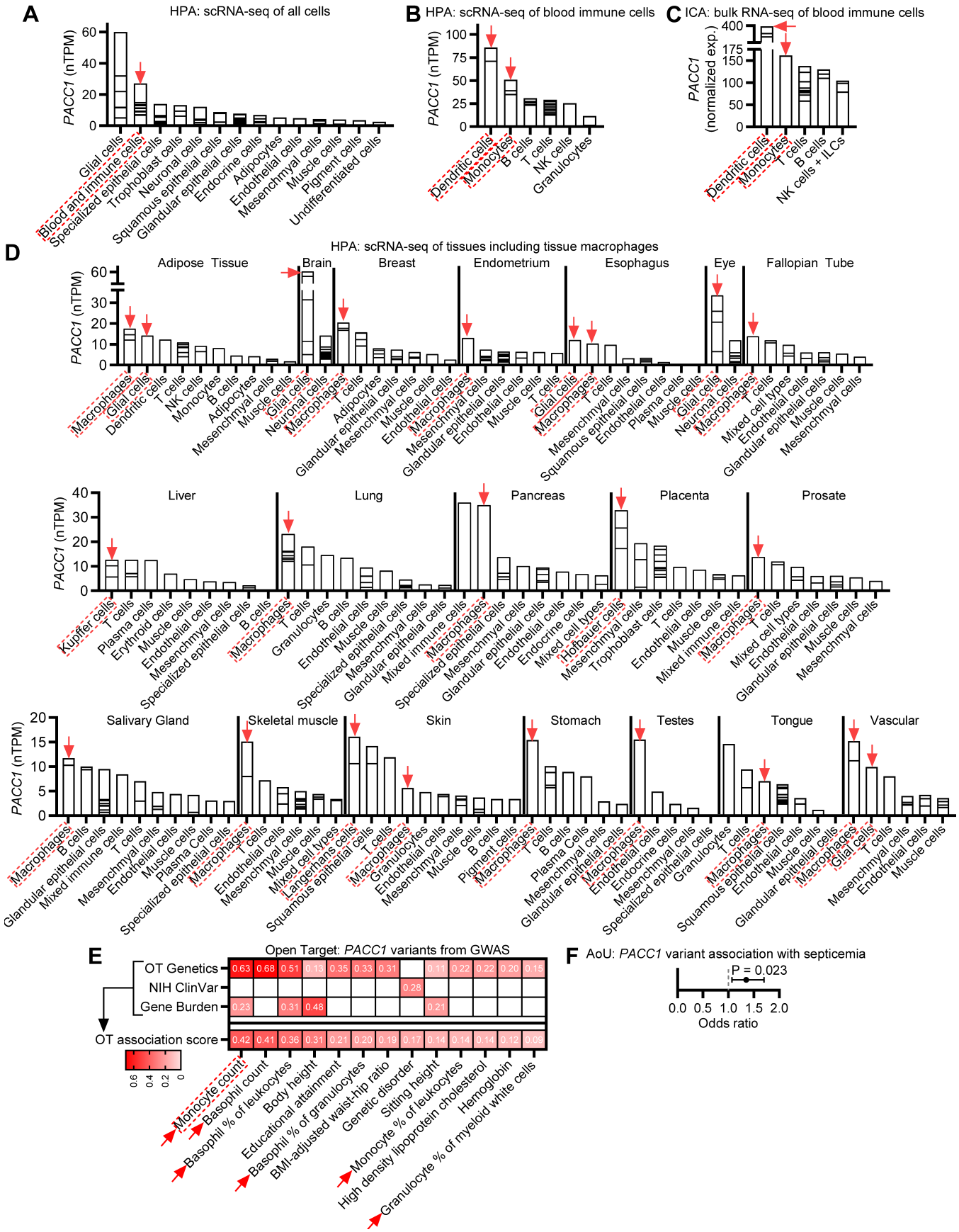
A
HPA: scRNA-seq of all cells
PACC1 (nTPM)
Glial cells
Blood and immune cells
Specialized epithelial cells
Trophoblast cells
Neuronal cells
Squamous epithelial cells
Glandular epithelial cells
Endocrine cells
Adipocytes
Endothelial cells
Mesenchymal cells
Muscle cells
Pigment cells
Undifferentiated cells
B
HPA: scRNA-seq of blood immune cells
Dendritic cells
Monocytes
B cells
T cells
NK cells
Granulocytes
C
ICA: bulk RNA-seq of blood immune cells
PACC1 (normalized exp.)
Dendritic cells
Monocytes
T cells
B cells
NK cells + ILCs
D
HPA: scRNA-seq of tissues including tissue macrophages
Adipose Tissue
Brain
Breast
Endometrium
Esophagus
Eye
Fallopian Tube
Liver
Lung
Pancreas
Placenta
Prosate
Salivary Gland
Skeletal muscle
Skin
Stomach
Testes
Tongue
Vascular
E
Open Target: PACC1 variants from GWAS
OT Genetics
NIH ClinVar
Gene Burden
OT association score
Monocyte count
Basophil count
Basophil % of leukocytes
Body height
Educational attainment
Basophil % of granulocytes
BMI-adjusted waist-hip ratio
Genetic disorder
Sitting height
Monocyte % of leukocytes
High density lipoprotein cholesterol
Hemoglobin
Granulocyte % of myeloid white cells
F
AoU: PACC1 variant association with septicemia
P = 0.023
Odds ratio

Fig. 1. *PACC1* expression is enriched in human mononuclear phagocytes, particularly tissue macrophages, and *PACC1* variants are implicated in myeloid cell-mediated immunity

A-D Data from single-cell RNA sequencing (scRNA-seq) studies in the Human Protein Atlas (HPA) or bulk RNA-seqstudies in the ImmGen Immune Cell Atlas (ICA), as indicated. Curated cell types along the x-axis contain *superimposed* (not stacked) data from cells (HPA) or sorted cell subsets (ICA) that were clustered and annotated, such that each horizontal line on the bar graphs represents the gene expression for an individual cell type or cluster. For the HPA, data are normalized transcripts per million (nTPM), corresponding to mean values of the different individual samples from each cell type. The ICA data represent mean values of normalized counts from different individual samples. (**A**) *PACC1* expression in all annotated somatic human cell types from the HPA. Red arrows/boxes indicate cells of interest (i.e., immune cells). (**B**) *PACC1* expression in blood immune cells from the HPA. Red arrows/boxes indicate cells of interest (i.e., mononuclear phagocytes). (**C**) *PACC1* expression in blood immune cells from the ICA. Red arrows/boxes indicate cells of interest (i.e., mononuclear phagocytes). (**D**) *PACC1* expression in all 19 somatic tissues from the HPA wherein tissue macrophages were detected and annotated. Cell clusters are broadly curated in combined bars (e.g., epithelial cells, endothelial cells), while immune cell clusters are in separate bars at greater resolution (e.g., macrophages, granulocytes). Red arrows/boxes indicate cells of interest (i.e., macrophages). (**E**) Heatmap ranking showing the most well-evidenced *PACC1* genetic variant associations across all observed phenotypes, according to the Open Targets Platform for genome-wide association studies (GWAS), ranked by “association scores” which synthesize evidence across databases (e.g., OT Genetics, NIH ClinVar, Gene Burden). Red arrows/boxes indicate *PACC1* variant associations with phenotypes of interest (i.e., myeloid cell-related phenotypes). (**F**) Forest plot showing association between gene-level predicted loss-of-function variant burden (low, rare and ultra rare, minor allele frequency <1%) in *PACC1* with septicemia phecode in the AoU dataset. The plot shows burden test P-value, odds ratio, and 95% confidence interval.

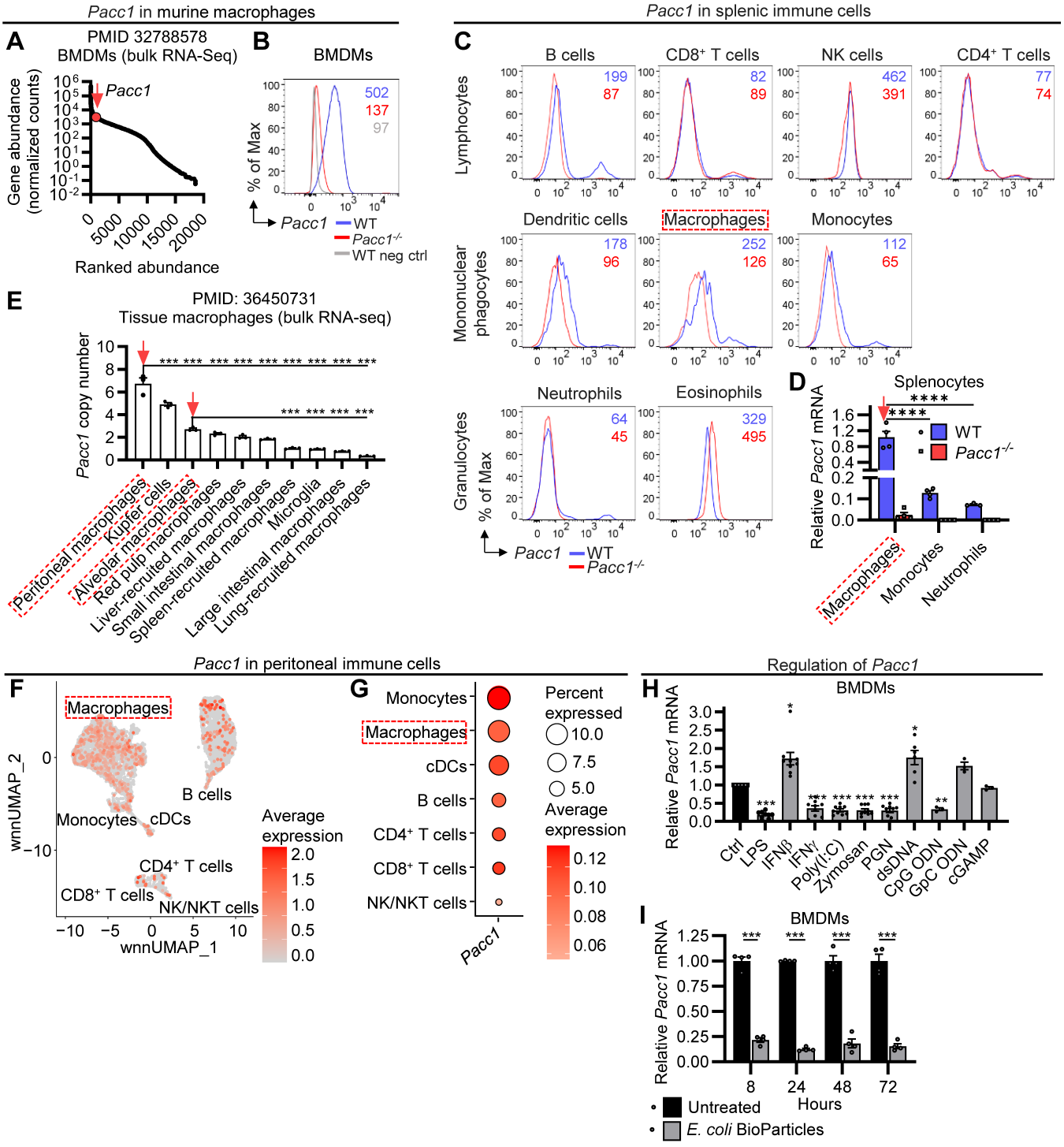
Pacc1 in murine macrophages
A
PMID 32788578
BMDMs (bulk RNA-Seq)
Gene abundance (normalized counts)
Pacc1
Ranked abundance
B
BMDMs
% of Max
502
137
97
Pacc1
WT
Pacc1-/-
WT neg ctrl
E
PMID: 36450731
Tissue macrophages (bulk RNA-seq)
Pacc1 copy number
Peritoneal macrophages
Kupffer cells
Alveolar macrophages
Red pulp macrophages
Liver-recruited macrophages
Small intestinal macrophages
Spleen-recruited macrophages
Microglia
Large intestinal macrophages
Lung-recruited macrophages
Pacc1 in splenic immune cells
C
Lymphocytes
B cells
CD8+ T cells
NK cells
CD4+ T cells
Mononuclear phagocytes
Dendritic cells
Macrophages
Monocytes
Granulocytes
Neutrophils
Eosinophils
% of Max
Pacc1
WT
Pacc1-/-
D
Splenocytes
Relative Pacc1 mRNA
WT
Pacc1-/-
Macrophages
Monocytes
Neutrophils
Pacc1 in peritoneal immune cells
F
Macrophages
B cells
Monocytes
cDCs
CD4+ T cells
CD8+ T cells
NK/NKT cells
wnnUMAP_1
wnnUMAP_2
Average expression
G
Monocytes
Macrophages
cDCs
B cells
CD4+ T cells
CD8+ T cells
NK/NKT cells
Pacc1
Percent expressed
Average expression
Regulation of Pacc1
H
BMDMs
Relative Pacc1 mRNA
Ctrl
LPS
IFNβ
IFNγ
Poly(I:C)
Zymosan
PGN
dsDNA
CpG ODN
GpC ODN
cGAMP
I
BMDMs
Relative Pacc1 mRNA
Hours
Untreated
E. coli BioParticles

Fig. 2. *Pacc1* expression is highly expressed in murine macrophages and other mononuclear phagocytes.

(**A**) Ranked gene expression of bulk RNA sequencing (bulk RNA-seq) data of bone marrow-derived macrophages (BMDMs) isolated *ex vivo* from wildtype (WT) mice. Data reanalyzed from our previous study (Roewe *et al. (12)*). *Pacc1* expression is shown in red in the top 5%. (**B-D**) *Pacc1* fluorescence intensities, representing mRNA gene expression, in representative flow cytometric histograms by RNA PrimeFlow staining in immune cells from WT or *Pacc1* knockout (*Pacc1*$^{-/-}$) mice. Data represent 2 independent experiments. Red arrows/boxes indicate cells of interest (i.e., macrophages). (**B**) Representative flow cytometric histograms of *Pacc1* expression in resting bone marrow-derived macrophages (BMDMs). Neg ctrl indicates no target probe. Geometric mean fluorescence intensities (MFIs) are indicated in the upper right. (**C**) Representative flow cytometric histograms with MFIs of *Pacc1* expression in splenocytes. (**D**) *Pacc1* expression in selected FACSorted splenocyte myeloid populations (live CD11b^{+}F4/80^{+} macrophages, CD11b^{+}Ly6C^{+}Ly6G^{-} monocytes, and CD11b^{+}Ly6C^{+}Ly6G^{+} neutrophils) by RT-qPCR normalized to WT macrophage expression. Red arrows/boxes indicate cells of interest (i.e., macrophages). (**E**) *Pacc1* copy number in bulk RNA-seq data from tissue macrophages isolated from WT mice. Data reanalyzed from Qie *et al.* (50). Red arrows/boxes indicate tissue macrophages of interest. (**F-G**) *Pacc1* expression by single-nucleus RNA sequencing of peritoneal cells from WT mice. Red boxes indicate cells of interest (i.e., macrophages). (**F**) *Pacc1* expression in annotated immune cell clusters visualized on the weight-nearest neighbor uniform manifold approximation and projection (wnnUMAP) plot. (**G**) Dot plot of *Pacc1* expression, where dot size indicates the percentage of cells expressing *Pacc1*, while color scale represents average *Pacc1* mRNA expression. (**H**) *Pacc1* expression in stimulated WT BMDMs analyzed by RT-qPCR, normalized to untreated control. In brief, BMDMs were stimulated for 24 h with various stimuli corresponding to inflammatory or infectious insults, including LPS (100 ng/mL), IFN-β (500 U/mL), IFN-ɣ (100 ng/mL), poly I:C (1 μg/mL), zymosan (10 μg/mL), PGN (10 μg/mL), dsDNA (1 μg/mL), CpG ODN (1 μM), GpC ODN (1 μM), or cGAMP (10 μg/mL). dsDNA was transfected using oligofectamine. Abbreviations: cGAMP, cyclic guanosine monophosphate–adenosine

monophosphate; dsDNA, double-stranded DNA; IFN-β, interferon beta; IFN-ɣ, interferon gamma; ODN, oligodeoxynucleotides; LPS, lipopolysaccharide; PGN, peptidoglycan; poly I:C, polyinosinic:polycytidylic acid. (**I**) *Pacc1* expression in BMDMs stimulated with inactivated *E. coli* Bioparticles (1:10 dilution) for the indicated time points analyzed by RT-qPCR, normalized to untreated control at each time point. For **B**-**D**, **H**, **I**, data represent ≥2 independent experiments. For **D**, **E**, **H**, **I**, data show one symbol per mouse, mean±SEM, *P<0.05, **P<0.01, ***P<0.001, ****P<0.0001,one-way ANOVA with Tukey (**D**), one-way ANOVA with Sidak (**E**, **I**), two-way ANOVA with Tukey (**D**), or one-way ANOVA with Dunett comparing each condition to unstimulated control (**H**).

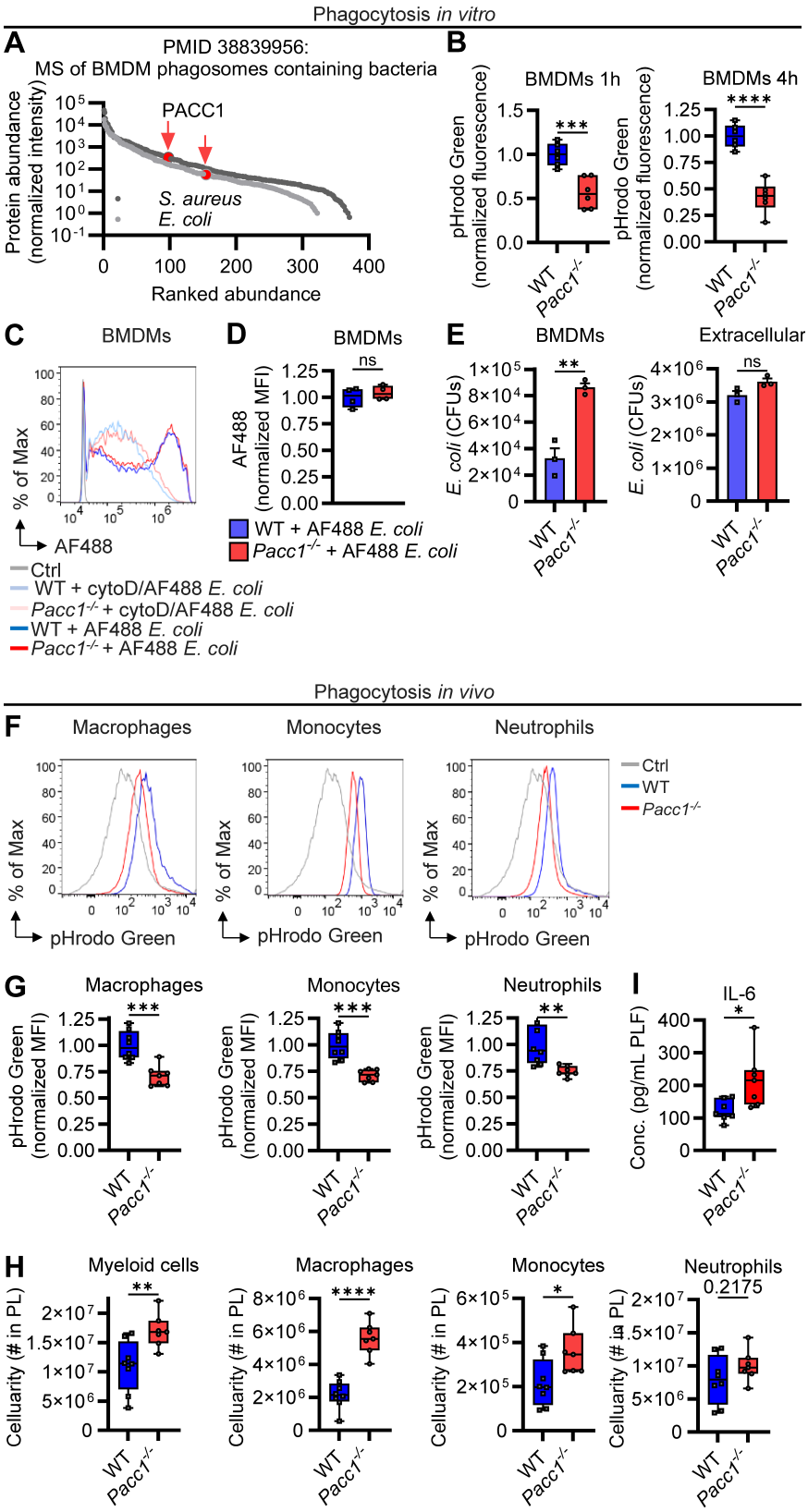
Phagocytosis in vitro
A
PMID 38839956:
MS of BMDM phagosomes containing bacteria
Protein abundance (normalized intensity)
PACC1
S. aureus
E. coli
Ranked abundance
B
BMDMs 1h
BMDMs 4h
pHrodo Green (normalized fluorescence)
***
****
WT
Pacc1-/-
C
BMDMs
% of Max
AF488
Ctrl
WT + cytoD/AF488 E. coli
Pacc1-/- + cytoD/AF488 E. coli
WT + AF488 E. coli
Pacc1-/- + AF488 E. coli
D
BMDMs
AF488 (normalized MFI)
ns
WT + AF488 E. coli
Pacc1-/- + AF488 E. coli
E
BMDMs
Extracellular
E. coli (CFUs)
**
ns
Phagocytosis in vivo
F
Macrophages
Monocytes
Neutrophils
% of Max
pHrodo Green
Ctrl
WT
Pacc1-/-
G
Macrophages
Monocytes
Neutrophils
pHrodo Green (normalized MFI)
***
***
**
I
IL-6
Conc. (pg/mL PLF)
*
H
Myeloid cells
Macrophages
Monocytes
Neutrophils
Celluarity (# in PL)
**
****
*
0.2175

Fig. 3. *Pacc1*$^{-/-}$ mice have defective development of the acidifying phagolysosome.

(**A**) Ranked protein abundance from mass spectrometry (MS) data of the phagosomes of bone-marrow-derived macrophages (BMDMs) stimulated with bacteria. Data reanalyzed from Li *et al.* (52). In brief, BMDMs were stimulated with ascorbate peroxidase (APEX)-modified inactivated bacteria followed by ascorbate peroxidase-mediated proximity ligation, and subsequently mass spectrometry was performed to identify phagosomal proteins proximal to phagocytosed bacteria. PACC1 is highlighted in red. (**B**) Wildtype (WT) and *Pacc1*$^{-/-}$ BMDMs were treated with 330 µg/mL acid-sensitive pHrodo Green *E. coli* BioParticles for the indicated time points. Fluorescence was measured by plate-reader and normalized to WT for each time point to assay development of phagolysosomal acidification. (**C-D**) WT and *Pacc1*$^{-/-}$ BMDMs were treated with acid-insensitive Alexa Fluor (AF)488 *E. coli* BioParticles. After 1 h, AF488 geometric mean fluorescence intensity (MFI) was measured by flow cytometry to assay phagocytic uptake. (**C**) Representative flow cytometric histograms of live BMDMs are shown. Cyto D indicates negative control cells that were pre-treated with the actin inhibitor, cytochalasin D, for 1 hour at 10µM to limit phagocytic uptake. Ctrl indicates negative control WT cells that were treated with inactivated *E. coli* without conjugation of fluorescent particles. (**D**) MFI quantifications from panel **C**, normalized to WT. (**E**) Colony-forming unit (CFU) counts from WT and *Pacc1*$^{-/-}$ BMDMs infected with pathogenic *E. coli* serotype O6:K2:H1 at an MOI of 5 for 2 h, followed by determination of CFUs in macrophage lysates and extracellular supernatants via serially diluted plated cultures, to assay bacterial killing capacity. (**F-I**) WT and *Pacc1*$^{-/-}$ mice were injected i.p. with 100 µg pHrodo Green *E. coli* BioParticles. After 24 h, cellularity and pHrodo Green MFI were measured by flow cytometry to assay development of phagolysosomal acidification from cells in peritoneal lavage. (**F**) Representative flow cytometric histograms of live CD11b^{+}Ly6C$^{-/lo}$F4/80^{+} macrophages, CD11b^{+}Ly6C^{hi}Ly6G^{-} monocytes, and CD11b^{+}Ly6C^{+}Ly6G^{+} neutrophils are shown. Ctrl indicates baseline fluorescence of total live cells from an unstimulated WT mouse. (**G**) MFI quantifications from panel **F**, normalized to WT. (**H**) Cell numbers from the peritoneal lavage (PL) of the same *E. coli* BioParticle experiments described above, including cell counts of total live CD11b^{+} myeloid cells, assessed by flow cytometry. (**I**) IL-6 concentration in peritoneal lavage fluid

(PLF) by ELISA from the same *E. coli* BioParticle experiments described above. For **B**-**I**, data represent ≥2 independent experiments. For **B**, **D**, **E**, **G**-**I**, data show one symbol per mouse. Bar graphs depict mean±SEM, and box plots show median and interquartile range with whiskers extended to the minimum and maximum. *P<0.05, **P<0.01, ***P<0.001, ****P<0.0001, ns=not significant, Student's t-test.

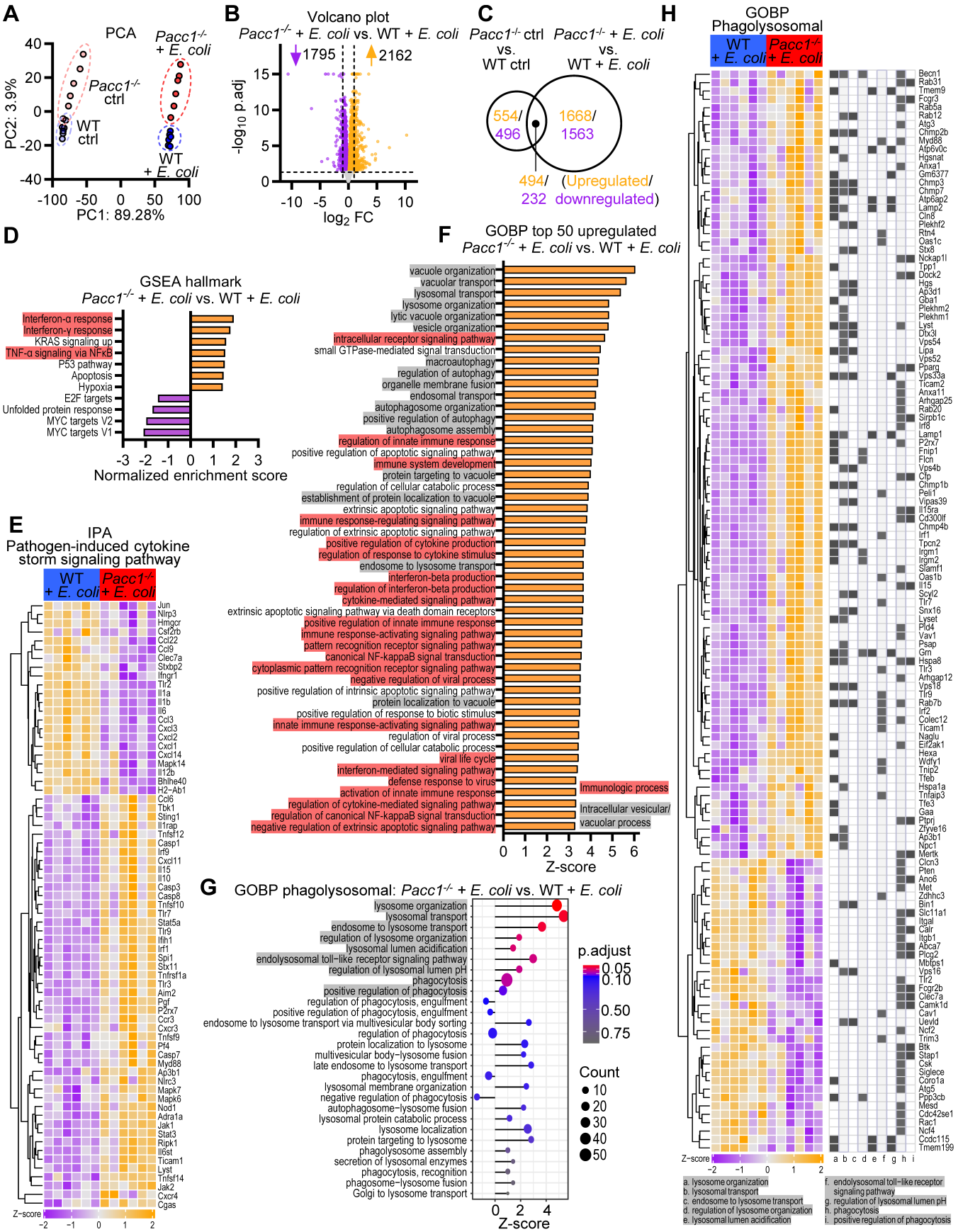
A
PCA
Pacc1-/- + E. coli
Pacc1-/- ctrl
WT ctrl
WT + E. coli
PC2: 3.9%
PC1: 89.28%
B
Volcano plot
Pacc1-/- + E. coli vs. WT + E. coli
1795
2162
-log10 p.adj
log2 FC
C
Pacc1-/- ctrl vs. WT ctrl
Pacc1-/- + E. coli vs. WT + E. coli
554/ 496
1668/ 1563
494/ 232
(Upregulated/ downregulated)
D
GSEA hallmark
Pacc1-/- + E. coli vs. WT + E. coli
Interferon-α response
Interferon-γ response
KRAS signaling up
TNF-α signaling via NFκB
P53 pathway
Apoptosis
Hypoxia
E2F targets
Unfolded protein response
MYC targets V2
MYC targets V1
Normalized enrichment score
E
IPA
Pathogen-induced cytokine storm signaling pathway
WT + E. coli
Pacc1-/- + E. coli
Z-score
F
GOBP top 50 upregulated
Pacc1-/- + E. coli vs. WT + E. coli
vacuole organization
vacuolar transport
lysosomal transport
lysosome organization
lytic vacuole organization
vesicle organization
intracellular receptor signaling pathway
small GTPase-mediated signal transduction
macroautophagy
regulation of autophagy
organelle membrane fusion
endosomal transport
autophagosome organization
positive regulation of autophagy
autophagosome assembly
regulation of innate immune response
positive regulation of apoptotic signaling pathway
immune system development
protein targeting to vacuole
regulation of cellular catabolic process
establishment of protein localization to vacuole
extrinsic apoptotic signaling pathway
immune response-regulating signaling pathway
regulation of extrinsic apoptotic signaling pathway
positive regulation of cytokine production
regulation of response to cytokine stimulus
endosome to lysosome transport
interferon-beta production
regulation of interferon-beta production
cytokine-mediated signaling pathway
extrinsic apoptotic signaling pathway via death domain receptors
positive regulation of innate immune response
immune response-activating signaling pathway
pattern recognition receptor signaling pathway
canonical NF-kappaB signal transduction
cytoplasmic pattern recognition receptor signaling pathway
negative regulation of viral process
positive regulation of intrinsic apoptotic signaling pathway
protein localization to vacuole
positive regulation of response to biotic stimulus
innate immune response-activating signaling pathway
regulation of viral process
positive regulation of cellular catabolic process
viral life cycle
interferon-mediated signaling pathway
defense response to virus
activation of innate immune response
regulation of cytokine-mediated signaling pathway
regulation of canonical NF-kappaB signal transduction
negative regulation of extrinsic apoptotic signaling pathway
Immunologic process
Intracellular vesicular/ vacuolar process
Z-score
G
GOBP phagolysosomal: Pacc1-/- + E. coli vs. WT + E. coli
lysosome organization
lysosomal transport
endosome to lysosome transport
regulation of lysosome organization
lysosomal lumen acidification
endolysosomal toll-like receptor signaling pathway
regulation of lysosomal lumen pH
phagocytosis
positive regulation of phagocytosis
regulation of phagocytosis, engulfment
positive regulation of phagocytosis, engulfment
endosome to lysosome transport via multivesicular body sorting
regulation of phagocytosis
protein localization to lysosome
multivesicular body-lysosome fusion
late endosome to lysosome transport
phagocytosis, engulfment
lysosomal membrane organization
negative regulation of phagocytosis
autophagosome-lysosome fusion
lysosomal protein catabolic process
lysosome localization
protein targeting to lysosome
phagolysosome assembly
secretion of lysosomal enzymes
phagocytosis, recognition
phagosome-lysosome fusion
Golgi to lysosome transport
p.adjust
Count
Z-score
H
GOBP Phagolysosomal
WT + E. coli
Pacc1-/- + E. coli
Z-score
a. lysosome organization
b. lysosomal transport
c. endosome to lysosome transport
d. regulation of lysosome organization
e. lysosomal lumen acidification
f. endolysosomal toll-like receptor signaling pathway
g. regulation of lysosomal lumen pH
h. phagocytosis
i. positive regulation of phagocytosis

Fig. 4. Transcriptomic profiling of dysregulated immunologic and phagolysosomal pathways in bone marrow-derived macrophages (BMDMs) from *Pacc1*$^{-/-}$ mice and wildtype mice stimulated with *E. coli* Bioparticles.

Wildtype (WT) and *Pacc1*$^{-/-}$ BMDMs were stimulated with *E. coli* BioParticles at 100 µg/mL or left as unstimulated controls (ctrl) for 12 h and subjected to bulk RNA sequencing (n=6 mice/group). (**A**) Principal component analysis (PCA) plot of the top 5000 variable genes after variance-stabilizing transformation of RNA sequencing counts from WT and *Pacc1*$^{-/-}$ BMDMs with *E. coli* or as unstimulated controls. PCA displays *E. coli*-dependent and genotype-dependent distinct clusters. (**B**) Volcano plot of differentially expressed genes (DEGs) in *Pacc1*$^{-/-}$ vs. WT BMDMs following *E. coli* incubation. Dotted lines indicate adj. P=0.05 and absolute $\log_2$ fold change (FC) =1; and values for $-\log_{10}$ adj. P>15 were set to 15 for visualization. (**C**) Venn diagram showing common and specific significant DEGs in *Pacc1*$^{-/-}$ vs. WT BMDMs with *E. coli* or as unstimulated controls. (**D**) Bar plot showing hallmark gene set enrichment analysis (GSEA) results in *Pacc1*$^{-/-}$ vs. WT BMDMs with *E. coli*. Immunologic pathways are highlighted in red. (**E**) Heatmap of significant DEGs enriched in "Pathogen Induced Cytokine Storm Signaling Pathway" from Ingenuity Pathway Analysis (IPA) in *Pacc1*$^{-/-}$ vs. WT BMDMs with *E. coli*. Normalized expression values. (**F**) Bar plot showing top 50 significant (adj. P<0.1) positively enriched gene ontology biological processes (GOBPs) in *Pacc1*$^{-/-}$ vs. WT BMDMs with *E. coli*. Immunologic pathways are highlighted in red, and intracellular vesicular/vacuolar pathways in gray. (**G**) Lollipop plot of manually curated phagolysosomal GOBPs showing both enriched (adj. P<0.1) and non-enriched in *Pacc1*$^{-/-}$ vs. WT BMDMs with *E. coli*. (**H**) Heatmap of significant DEGs within enriched (adj. P<0.1) phagolysosomal GOBPs from panel **G** in *Pacc1*$^{-/-}$ vs. WT BMDMs with *E. coli*. Genes enriched within each GOBP are indicated within the shaded squares. Heatmaps show normalized expression values with Z-score from -2/purple to +2/orange and statistical significance for DEGs at adj. P<0.05. See also ***SI Appendix,* Datasets 1–4**.

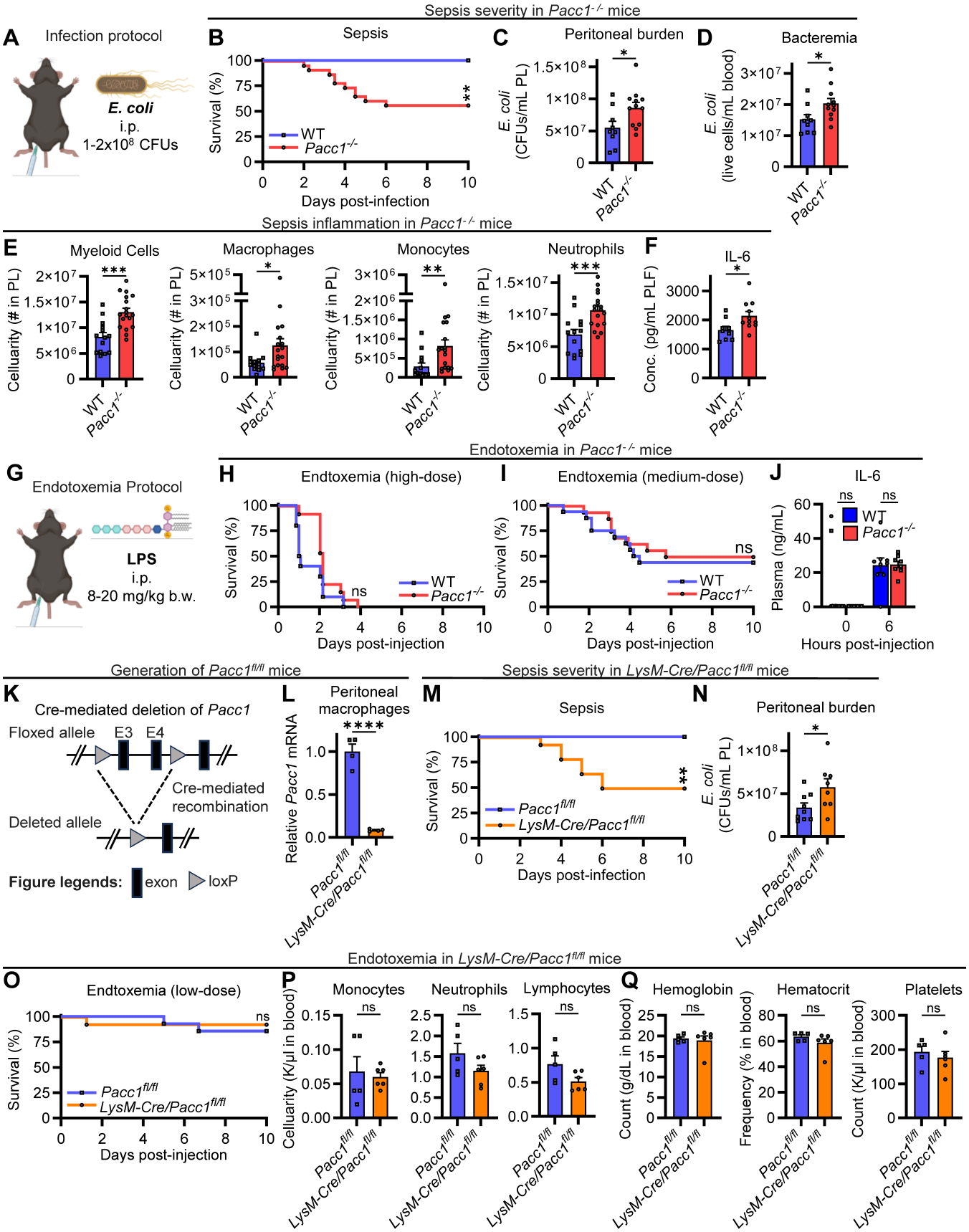
Sepsis severity in Pacc1-/- mice
A
Infection protocol
E. coli
i.p.
1-2x10^8 CFUs
B
Sepsis
Survival (%)
WT
Pacc1-/-
Days post-infection
C
Peritoneal burden
E. coli (CFUs/mL PL)
D
Bacteremia
E. coli (live cells/mL blood)
Sepsis inflammation in Pacc1-/- mice
E
Myeloid Cells
Macrophages
Monocytes
Neutrophils
Celluarity (# in PL)
F
IL-6
Conc. (pg/mL PLF)
Endotoxemia in Pacc1-/- mice
G
Endotoxemia Protocol
LPS
i.p.
8-20 mg/kg b.w.
H
Endtoxemia (high-dose)
I
Endtoxemia (medium-dose)
J
IL-6
Plasma (ng/mL)
Hours post-injection
Generation of Pacc1fl/fl mice
K
Cre-mediated deletion of Pacc1
Floxed allele
E3
E4
Cre-mediated recombination
Deleted allele
Figure legends:
exon
loxP
L
Peritoneal macrophages
Relative Pacc1 mRNA
Pacc1fl/fl
LysM-Cre/Pacc1fl/fl
Sepsis severity in LysM-Cre/Pacc1fl/fl mice
M
Sepsis
N
Peritoneal burden
Endotoxemia in LysM-Cre/Pacc1fl/fl mice
O
Endtoxemia (low-dose)
P
Monocytes
Neutrophils
Lymphocytes
Celluarity (K/µl in blood)
Q
Hemoglobin
Count (g/dL in blood)
Hematocrit
Frequency (% in blood)
Platelets
Count (K/µl in blood)

Fig. 5. Global and myeloid cell conditional *Pacc1* deletion confers susceptibility to *E. coli* sepsis. (**A**) Schematic showing sepsis infection protocol. Wildtype (WT) and *Pacc1*$^{-/-}$ mice were given 1-2x10^8 colony-forming units (CFUs) of *Escherichia (E). coli* intraperitoneally (i.p.). Peritoneal lavage (PL) and blood were collected after 6 or 24 h, or survival was monitored, as indicated. (**B**) Sepsis survival (n=17-22 mice/group, pooled from 3 independent experiments). (**C**) CFUs in peritoneal lavage after 6 h of infection assayed by serially diluted plated cultures. (**D**) Number of live (propidium iodide negative) bacteria in blood after 24 h of infection measured by flow cytometry. (**E**) Myeloid cell numbers in peritoneal lavage after 24 h of infection assessed by flow cytometry. (**F**) IL-6 in peritoneal lavage fluid (PLF) after 6 h of infection by ELISA. (**G**) Schematic showing endotoxemia induction protocol. Mice were given *E. coli*-derived lipopolysaccharide (LPS) i.p. to induce phagocytosis-independent endotoxemia. (**H**) Endotoxemia survival with high-dose (20 mg/kg body weight [b.w.]) LPS (n=10-13 mice/group). (**I**) Endotoxemia survival with medium-dose (10 mg/kg b.w.) LPS (n=16 mice/group, 2 pooled experiments). (**J**) IL-6 in plasma after low-dose LPS endotoxemia as in panel H by ELISA. (**K**) Schematic showing generation of *Pacc1*-floxed mice and Cre-mediated deletion. In brief, LoxP sites flanking exons 3/4 of the *Pacc1* were inserted using CRISPR/Cas9 in WT mice, such that Cre-mediated deletion of these exons eliminates productive *Pacc1* expression. (**L**) *Pacc1* expression loss in live CD11b$^+$F4/80$^+$ peritoneal macrophages from *LysM-Cre/Pacc1*$^{fl/fl}$ mice by qRT-PCR. *Pacc1*-floxed (*Pacc1*$^{fl/fl}$) and *LysM-Cre* mice were crossed for targeted deletion of *Pacc1* in myeloid cells, and macrophages were sorted by flow cytometry from the lavages of naïve mice. (**M**) Sepsis survival following *E. coli* infection as in A (n=11-14 mice/group, pooled from 2 independent experiments). (**N**) CFUs in peritoneal lavage after 6 h of infection were measured by serially diluted plated cultures. (**O**) Endotoxemia survival with low-dose (8 mg/kg b.w.) LPS (n=14 mice/group). (**P**) Immune cell counts determined by blood analyzed in mice with low-dose endotoxemia after 24 h. (**Q**) Blood parameters determined by blood analyzer in mice with low-dose endotoxemia after 24 h. Data represent ≥2 independent experiments and show one symbol per mouse,

mean±SEM, *P<0.05, **P<0.01, ***P<0.001, ns=not significant, Student's t-test (**C-F, J**, **L**, **N**, **P**, **Q**), or Mantel-Cox log-rank test (**B**, **H**, **I**, **M**, **O**).

References

1. K. E. Rudd *et al.*, Global, regional, and national sepsis incidence and mortality, 1990-2017: analysis for the Global Burden of Disease Study. *Lancet* **395**, 200-211 (2020).
2. C. J. Paoli, M. A. Reynolds, M. Sinha, M. Gitlin, E. Crouser, Epidemiology and Costs of Sepsis in the United States-An Analysis Based on Timing of Diagnosis and Severity Level. *Crit Care Med* **46**, 1889-1897 (2018).
3. C. M. Torio, B. J. Moore, "National Inpatient Hospital Costs: The Most Expensive Conditions by Payer, 2013" in Healthcare Cost and Utilization Project (HCUP) Statistical Briefs. (Agency for Healthcare Research and Quality (US), Rockville (MD), 2006).
4. C. Rhee *et al.*, Prevalence, Underlying Causes, and Preventability of Sepsis-Associated Mortality in US Acute Care Hospitals. *JAMA Netw Open* **2**, e187571 (2019).
5. L. J. Quinton, A. J. Walkey, J. P. Mizgerd, Integrative Physiology of Pneumonia. *Physiol Rev* **98**, 1417-1464 (2018).
6. Anonymous, Global burden of bacterial antimicrobial resistance 1990-2021: a systematic analysis with forecasts to 2050. *Lancet* 10.1016/s0140-6736(24)01867-1 (2024).
7. E. Karakike *et al.*, Coronavirus Disease 2019 as Cause of Viral Sepsis: A Systematic Review and Meta-Analysis. *Crit Care Med* **49**, 2042-2057 (2021).
8. M. Bonten *et al.*, Epidemiology of Escherichia coli Bacteremia: A Systematic Literature Review. *Clin Infect Dis* **72**, 1211-1219 (2021).
9. Anonymous, Global mortality associated with 33 bacterial pathogens in 2019: a systematic analysis for the Global Burden of Disease Study 2019. *Lancet* **400**, 2221-2248 (2022).
10. S. Tereziu, D. A. Minter, "Pneumococcal Vaccine" in StatPearls. (StatPearls Publishing Copyright © 2023, StatPearls Publishing LLC., Treasure Island (FL), 2023).
11. M. Bosmann *et al.*, Interruption of macrophage-derived IL-27(p28) production by IL-10 during sepsis requires STAT3 but not SOCS3. *J Immunol* **193**, 5668-5677 (2014).
12. J. Roewe *et al.*, Bacterial polyphosphates interfere with the innate host defense to infection. *Nat Commun* **11**, 4035 (2020).
13. M. Bosmann, N. F. Russkamp, P. A. Ward, Fingerprinting of the TLR4-induced acute inflammatory response. *Exp Mol Pathol* **93**, 319-323 (2012).
14. M. Bosmann *et al.*, CD11c+ alveolar macrophages are a source of IL-23 during lipopolysaccharide-induced acute lung injury. *Shock* **39**, 447-452 (2013).
15. S. H. E. Kaufmann, A. Dorhoi, R. S. Hotchkiss, R. Bartenschlager, Host-directed therapies for bacterial and viral infections. *Nat Rev Drug Discov* **17**, 35-56 (2018).
16. M. Bosmann, P. A. Ward, The inflammatory response in sepsis. *Trends Immunol* **34**, 129-136 (2013).
17. E. Mass, F. Nimmerjahn, K. Kierdorf, A. Schlitzer, Tissue-specific macrophages: how they develop and choreograph tissue biology. *Nature Reviews Immunology* **23**, 563-579 (2023).
18. A. M. Pauwels, M. Trost, R. Beyaert, E. Hoffmann, Patterns, Receptors, and Signals: Regulation of Phagosome Maturation. *Trends Immunol* **38**, 407-422 (2017).
19. E. Uribe-Querol, C. Rosales, Phagocytosis: Our Current Understanding of a Universal Biological Process. *Front Immunol* **11**, 1066 (2020).
20. T. J. Jentsch, M. Pusch, CLC Chloride Channels and Transporters: Structure, Function, Physiology, and Disease. *Physiol Rev* **98**, 1493-1590 (2018).
21. T. Stauber, T. J. Jentsch, Chloride in vesicular trafficking and function. *Annu Rev Physiol* **75**, 453-477 (2013).
22. J. Yang *et al.*, PAC, an evolutionarily conserved membrane protein, is a proton-activated chloride channel. *Science* **364**, 395-399 (2019).
23. F. Ullrich *et al.*, Identification of TMEM206 proteins as pore of PAORAC/ASOR acid-sensitive chloride channels. *Elife* **8** (2019).

24. S. Lambert, J. Oberwinkler, Characterization of a proton-activated, outwardly rectifying anion channel. *J Physiol* **567**, 191-213 (2005).
25. C. Auzanneau, V. Thoreau, A. Kitzis, F. Becq, A Novel voltage-dependent chloride current activated by extracellular acidic pH in cultured rat Sertoli cells. *J Biol Chem* **278**, 19230-19236 (2003).
26. H. Y. Wang, T. Shimizu, T. Numata, Y. Okada, Role of acid-sensitive outwardly rectifying anion channels in acidosis-induced cell death in human epithelial cells. *Pflugers Arch* **454**, 223-233 (2007).
27. Z. Ruan, J. Osei-Owusu, J. Du, Z. Qiu, W. Lü, Structures and pH-sensing mechanism of the proton-activated chloride channel. *Nature* **588**, 350-354 (2020).
28. J. Osei-Owusu *et al.*, Molecular determinants of pH sensing in the proton-activated chloride channel. *Proc Natl Acad Sci U S A* **119**, e2200727119 (2022).
29. C. Wang, M. M. Polovitskaya, B. D. Delgado, T. J. Jentsch, S. B. Long, Gating choreography and mechanism of the human proton-activated chloride channel ASOR. *Sci Adv* **8**, eabm3942 (2022).
30. Z. Deng *et al.*, Cryo-EM structure of a proton-activated chloride channel TMEM206. *Sci Adv* **7** (2021).
31. J. Osei-Owusu, J. Yang, M. Del Carmen Vitery, M. Tian, Z. Qiu, PAC proton-activated chloride channel contributes to acid-induced cell death in primary rat cortical neurons. *Channels (Austin)* **14**, 53-58 (2020).
32. X. M. Zha, Z. G. Xiong, R. P. Simon, pH and proton-sensitive receptors in brain ischemia. *J Cereb Blood Flow Metab* **42**, 1349-1363 (2022).
33. P. Xue *et al.*, Proton-Activated Chloride Channel Increases Endplate Porosity and Pain in a Mouse Spinal Degeneration Model. *J Clin Invest* 10.1172/jci168155 (2024).
34. J. E. DiCiccio, B. E. Steinberg, Lysosomal pH and analysis of the counter ion pathways that support acidification. *J Gen Physiol* **137**, 385-390 (2011).
35. J. Osei-Owusu *et al.*, Proton-activated chloride channel PAC regulates endosomal acidification and transferrin receptor-mediated endocytosis. *Cell Rep* **34**, 108683 (2021).
36. M. Zeziulia, S. Blin, F. W. Schmitt, M. Lehmann, T. J. Jentsch, Proton-gated anion transport governs macropinosome shrinkage. *Nat Cell Biol* **24**, 885-895 (2022).
37. K. H. Chen *et al.*, Loss of the proton-activated chloride channel in neurons impairs AMPA receptor endocytosis and LTD via endosomal hyper-acidification. *Cell Rep* **44**, 115302 (2025).
38. N. Koylass *et al.*, The Proton-Activated Chloride Channel Inhibits SARS-CoV-2 Spike Protein-Mediated Viral Entry Through the Endosomal Pathway. *J Cell Physiol* **240**, e70063 (2025).
39. G. Monaco *et al.*, RNA-Seq Signatures Normalized by mRNA Abundance Allow Absolute Deconvolution of Human Immune Cell Types. *Cell Rep* **26**, 1627-1640.e1627 (2019).
40. T. S. Heng, M. W. Painter, The Immunological Genome Project: networks of gene expression in immune cells. *Nat Immunol* **9**, 1091-1094 (2008).
41. Y. J. Jung, W. S. Chung, Phagocytic Roles of Glial Cells in Healthy and Diseased Brains. *Biomol Ther (Seoul)* **26**, 350-357 (2018).
42. A. J. Byrne, S. A. Mathie, L. G. Gregory, C. M. Lloyd, Pulmonary macrophages: key players in the innate defence of the airways. *Thorax* **70**, 1189-1196 (2015).
43. A. Madhvi, H. Mishra, G. R. Leisching, P. Z. Mahlobo, B. Baker, Comparison of human monocyte derived macrophages and THP1-like macrophages as in vitro models for M. tuberculosis infection. *Comp Immunol Microbiol Infect Dis* **67**, 101355 (2019).
44. C. Klijn *et al.*, A comprehensive transcriptional portrait of human cancer cell lines. *Nat Biotechnol* **33**, 306-312 (2015).
45. D. Ochoa *et al.*, The next-generation Open Targets Platform: reimagined, redesigned, rebuilt. *Nucleic Acids Res* **51**, D1353-d1359 (2023).
46. S. J. Jurgens *et al.*, Rare coding variant analysis for human diseases across biobanks and ancestries. *Nat Genet* **56**, 1811-1820 (2024).

47. C. Bycroft *et al.*, The UK Biobank resource with deep phenotyping and genomic data. *Nature* **562**, 203-209 (2018).
48. S. F. Pastore *et al.*, Biallelic inheritance in a single Pakistani family with intellectual disability implicates new candidate gene RDH14. *Sci Rep* **11**, 23113 (2021).
49. C. Lai, D. Stepniak, L. Sias, C. Funatake, A sensitive flow cytometric method for multi-parametric analysis of microRNA, messenger RNA and protein in single cells. *Methods* **134-135**, 136-148 (2018).
50. J. Qie *et al.*, Integrated proteomic and transcriptomic landscape of macrophages in mouse tissues. *Nature Communications* **13**, 7389 (2022).
51. S. Lykke-Andersen, T. H. Jensen, Nonsense-mediated mRNA decay: an intricate machinery that shapes transcriptomes. *Nature Reviews Molecular Cell Biology* **16**, 665-677 (2015).
52. K. Li *et al.*, Profiling phagosome proteins identifies PD-L1 as a fungal-binding receptor. *Nature* **630**, 736-743 (2024).
53. A. Neaga, J. Lefor, K. E. Lich, S. F. Liparoto, Y. Q. Xiao, Development and validation of a flow cytometric method to evaluate phagocytosis of pHrodo™ BioParticles® by granulocytes in multiple species. *J Immunol Methods* **390**, 9-17 (2013).
54. B. Lindner, T. Burkard, M. Schuler, Phagocytosis assays with different pH-sensitive fluorescent particles and various readouts. *Biotechniques* **68**, 245-250 (2020).
55. C. Lambert *et al.*, Cytochalasans and Their Impact on Actin Filament Remodeling. *Biomolecules* **13** (2023).
56. I. Rusinova *et al.*, Interferome v2.0: an updated database of annotated interferon-regulated genes. *Nucleic Acids Res* **41**, D1040-1046 (2013).
57. M. Dudek *et al.*, Lung epithelium and myeloid cells cooperate to clear acute pneumococcal infection. *Mucosal Immunol* **9**, 1288-1302 (2016).
58. J. C. Gomez *et al.*, Mechanisms of interferon-γ production by neutrophils and its function during Streptococcus pneumoniae pneumonia. *Am J Respir Cell Mol Biol* **52**, 349-364 (2015).
59. C. L. Abram, G. L. Roberge, Y. Hu, C. A. Lowell, Comparative analysis of the efficiency and specificity of myeloid-Cre deleting strains using ROSA-EYFP reporter mice. *J Immunol Methods* **408**, 89-100 (2014).
60. H. Y. Cheng *et al.*, Proton-activated chloride channel governs phagosome-mediated antibacterial immunity in peritoneal macrophages. *J Exp Med* **222** (2025).
61. B. E. Steinberg *et al.*, A cation counterflux supports lysosomal acidification. *J Cell Biol* **189**, 1171-1186 (2010).
62. S. Weinert *et al.*, Uncoupling endosomal CLC chloride/proton exchange causes severe neurodegeneration. *Embo j* **39**, e103358 (2020).
63. A. Lukasiak, M. Zajac, The Distribution and Role of the CFTR Protein in the Intracellular Compartments. *Membranes* **11**, 804 (2021).
64. A. Meoli *et al.*, Impact of CFTR Modulators on the Impaired Function of Phagocytes in Cystic Fibrosis Lung Disease. *Int J Mol Sci* **23** (2022).
65. A. Badr *et al.*, CFTR Modulators Restore Acidification of Autophago-Lysosomes and Bacterial Clearance in Cystic Fibrosis Macrophages. *Front Cell Infect Microbiol* **12**, 819554 (2022).
66. W. McAlpine *et al.*, Excessive endosomal TLR signaling causes inflammatory disease in mice with defective SMCR8-WDR41-C9ORF72 complex function. *Proc Natl Acad Sci U S A* **115**, E11523-e11531 (2018).
67. O. de Bouteiller *et al.*, Recognition of double-stranded RNA by human toll-like receptor 3 and downstream receptor signaling requires multimerization and an acidic pH. *J Biol Chem* **280**, 38133-38145 (2005).
68. R. Siebeler, M. P. J. de Winther, M. A. Hoeksema, The regulatory landscape of macrophage interferon signaling in inflammation. *J Allergy Clin Immunol* **152**, 326-337 (2023).

69. J. H. Zhang, Y. Qin, S. C. Sun, TMEM206 gene knockout improves balance performance in SCA1 transgenic mice. *IBRO Neurosci Rep* **19**, 996-999 (2025).
70. S. Kappel *et al.*, CBA (4-chloro-2-(2-chlorophenoxy)acetamido) benzoic acid) inhibits TMEM206 mediated currents and TMEM206 does not contribute to acid-induced cell death in colorectal cancer cells. *Front Pharmacol* **15**, 1369513 (2024).
71. K. Melek, B. Hauert, S. Kappel, TMEM206 Contributes to Cancer Hallmark Functions in Colorectal Cancer Cells and Is Regulated by p53 in a p21-Dependent Manner. *Cells* **13** (2024).
72. F. Peng, H. Li, J. Li, Z. Wang, Downregulation of the Proton-Activated Cl- Channel TMEM206 Inhibits Malignant Properties of Human Osteosarcoma Cells. *Oxid Med Cell Longev* **2021**, 3672112 (2021).
73. L. Song, D. Feng, J. Tan, H. Zhang, Effects of TMEM206 on the malignant behavior of HepG2 human hepatocellular carcinoma cells. *European Journal of Inflammation* **20**, 1721727X221122724 (2022).
74. L. Zhang, S. Y. Liu, X. Yang, Y. Q. Wang, Y. X. Cheng, TMEM206 is a potential prognostic marker of hepatocellular carcinoma. *Oncol Lett* **20**, 174 (2020).
75. Z. J. Yang, S. Y. Huang, Y. F. Zhou, S. C. Sun, Knockout of TMEM206 in mice associated with a loss of corneal transparency. *Int J Ophthalmol* **17**, 1967-1972 (2024).
76. S. Gururaja Rao, N. J. Patel, H. Singh, Intracellular Chloride Channels: Novel Biomarkers in Diseases. *Front Physiol* **11**, 96 (2020).
77. S. Gururaja Rao, D. Ponnalagu, N. J. Patel, H. Singh, Three Decades of Chloride Intracellular Channel Proteins: From Organelle to Organ Physiology. *Curr Protoc Pharmacol* **80**, 11.21.11-11.21.17 (2018).
78. J. Osei-Owusu *et al.*, Molecular mechanism underlying desensitization of the proton-activated chloride channel PAC. *Elife* **11** (2022).
79. L. Mihaljević, Z. Ruan, J. Osei-Owusu, W. Lü, Z. Qiu, Inhibition of the proton-activated chloride channel PAC by PIP(2). *Elife* **12** (2023).
80. H. Y. Cheng *et al.*, The phagosome-mediated anti-bacterial immunity is governed by the proton-activated chloride channel in peritoneal macrophages. *bioRxiv* 10.1101/2025.02.27.640612, 2025.2002.2027.640612 (2025).
81. A. C. Ericsson, C. L. Franklin, The gut microbiome of laboratory mice: considerations and best practices for translational research. *Mamm Genome* **32**, 239-250 (2021).
82. V. M. Ripoll *et al.*, Nicotinamide nucleotide transhydrogenase (NNT) acts as a novel modulator of macrophage inflammatory responses. *Faseb j* **26**, 3550-3562 (2012).
83. K. H. Chen, T. Hagino, Z. Qiu, The Proton-Activated Chloride Channel: Molecular Identification, Structure, and Role in Organelle Physiology. *Annu Rev Physiol* 10.1146/annurev-physiol-022724-105357 (2025).
84. B. Boilly, A. S. Vercoutter-Edouart, H. Hondermarck, V. Nurcombe, X. Le Bourhis, FGF signals for cell proliferation and migration through different pathways. *Cytokine Growth Factor Rev* **11**, 295-302 (2000).